ELSEVIER

Coordination Chemistry Reviews
150 (1996) 131–161

COORDINATION CHEMISTRY REVIEWS

Chapter 5
Magnetic coupled systems

Contents

5.1. The induced magnetic moment per metal ion in polymetallic systems and the hyperfine contact shift

The compounds containing more than one metal ion with unpaired electrons deserve special attention because NMR is a powerful technique to relate the properties of the whole systems with those of each metal ion member. Magnetic coupling occurs when the spin magnetic moments of each metal ion interact with one another. The interaction is again quantized; for example, given S_1 and S_2 as two interacting spins, new spin levels are established, with total S' varying in unitary steps from $S_1 + S_2$ to $|S_1 - S_2|$. A major effect of magnetic spin coupling is the occurrence of new energy levels. Their energy separations are a function of J. In general, $|J|$ varies from almost zero to the order of $10^3\ cm^{-1}$. At any laboratory temperature, kT may be of the order of the above separation and so the problem of the temperature-dependent population of the levels is introduced. The population P_i of any spin level of energy E_i is given by

PII S0010-8545(96)01245-3

the Boltzmann law (Eq. (1.25)), which we recall here for convenience

$$P_i = \frac{\exp(-E_i/kT)}{\sum_i \exp(-E_i/kT)}$$

When kT is large with respect to the energy gap, the population of each level is just one over the number of levels or functions. When kT is small with respect to the energy separation, then only the lowest level is occupied. The new energy levels S' are linear combinations of the $|S, M_S\rangle$ functions of each metal ion. The functions and energies can be calculated by the simple Heisenberg Hamiltonian, that for a dimer is

$$\mathcal{H} = J\boldsymbol{S}_1 \cdot \boldsymbol{S}_2 \tag{5.1}$$

where J is a constant and $\boldsymbol{S}_1$ is the spin operator which operates only on the functions of metal 1 [1]. The eigenvalues of (5.1) are[1]

$$E = \frac{J}{2} S'(S'+1) \tag{5.2}$$

When J is positive, the ground state has $S' = |S_1 - S_2|$ and the highest level has $S' = S_1 + S_2$. We say that the coupling is antiferromagnetic. The contrary holds when J is negative and the coupling is ferromagnetic.

When more metal ions are coupled, the following Hamiltonian can be used:

$$\mathcal{H} = \sum_{j \neq k} J_{jk} \boldsymbol{S}_j \cdot \boldsymbol{S}_k \tag{5.3}$$

where all j–k pairwise interactions are taken into consideration. For each ith S', the contribution to the total induced magnetic moment is:

$$\langle \mu_i \rangle = -\mu_B g_e \langle S'_z \rangle_i P_i \tag{5.4}$$

the total induced magnetic moment being

$$\langle \mu \rangle = -\mu_B g_e \sum_i \langle S'_z \rangle_i P_i$$

The contact hyperfine shift experienced by a nucleus is proportional to the induced magnetic moment of each S' level times the hyperfine coupling constant

$$\delta^{\text{con}} = -\sum_i \frac{A_i}{h\gamma_I B_0} \langle S'_z \rangle_i P_i \tag{5.5}$$

This equation would be of little help if further considerations were not made. In fact, we do not know the several A_i values. However, the $|S', M_{S'}\rangle$ wavefunctions

[1] The eigenvalues of Eq. (5.1) can be derived by squaring the equality $\boldsymbol{S}' = \boldsymbol{S}_1 + \boldsymbol{S}_2$: $\boldsymbol{S}'^2 = \boldsymbol{S}_1^2 + \boldsymbol{S}_2^2 + 2\boldsymbol{S}_1 \cdot \boldsymbol{S}_2$ (since $\boldsymbol{S}_1$ and $\boldsymbol{S}_2$ commute) and, by rearranging, $\boldsymbol{S}_1 \cdot \boldsymbol{S}_2 = \frac{1}{2}[\boldsymbol{S}'^2 - \boldsymbol{S}_1^2 - \boldsymbol{S}_2^2]$. The eigenvalues of the Hamiltonian $J\boldsymbol{S}_1 \cdot \boldsymbol{S}_2$ are thus given by: $E = J/2[S'(S'+1) - S_1(S_1+1) - S_2(S_2+1)]$. Because $S_1(S_1+1)$ and $S_2(S_2+1)$ are the same for all S' levels, they introduce only an energy offset and can be dropped. The splitting of the levels is thus given by Eq. (5.2).

are linear combinations of the $|S, M_S\rangle$ wavefunctions of each metal ion; therefore we want to show that it is possible to express A_i through the hyperfine constant A_M of the single ions when they are not magnetically coupled. Let us assume that, without loss of generality, a nucleus senses only one metal ion of the cluster, M, i.e. it senses only the induced magnetic moment of that ion. If we are able to project out the $|S, M_S\rangle$ part for that metal from each $|S', M_{S'}\rangle$ wavefunction, then we can use the hyperfine constant A_M that the nucleus would experience if the metal ion were not involved in the magnetic coupling, i.e. if $J = 0$. Then the following relationship holds for each S' level:

$$A_i\langle S'_z\rangle_i = A_M\langle S_{Mz}\rangle_i \tag{5.6}$$

where $\langle S_{Mz}\rangle_i$ is the expectation value of the contribution of metal M to the whole wavefunction S'_i and $\langle S'_z\rangle_i$ is the usual expectation value of S'_z for each i level [2,3]. This relationship is based on the assumption that the establishment of magnetic interactions within a cluster does not change the spin density distribution on the ligands nor on the metal ion. This is apparently the case in the investigated systems. If $|J| \ll kT$, all the levels are equally populated and

$$\sum_i A_i\langle S'_z\rangle_i P_i = A_M \sum_i \langle S_{Mz}\rangle_i P_i = A_M\langle S_{Mz}\rangle \tag{5.7}$$

where $\langle S_{Mz}\rangle$ is the expectation value of S_z for metal M in the absence of magnetic interactions. It follows that the energy of interaction between a nucleus and the induced electronic magnetic moment sensed by it ($\propto A_M\langle S_{Mz}\rangle$) does not change upon establishment of magnetic coupling. The energy of interaction does change if only some of the S_i levels are occupied.

A useful formula to express the contact shift, in the case of a nucleus sensing only one metal ion, is

$$\delta^{con} = A_M \frac{g_e\mu_B}{h\gamma_I 3kT} \frac{\sum_i C_i S'_i(S'_i+1)(2S'_i+1)\exp(-E_i/kT)}{\sum_i (2S'_i+1)\exp(-E_i/kT)} \tag{5.8}$$

where

$$C_i = \langle S_{Mz}\rangle_i/\langle S'_z\rangle_i \tag{5.9}$$

If the nucleus senses another metal ion with a different A_M value, then the total shift will be given by the sum of two terms of the type of Eq. (5.8), each containing its own A_M and C_i values. A_{M1} and A_{M2} can be estimated from the monomeric analogs. The C_{i1} and C_{i2} values can be calculated once and for all for each system with the help of Hamiltonian (5.3). Their values are reported in Table 5.1 for dimers involving S_1 and S_2 values from $\frac{1}{2}$ to $\frac{7}{2}$ [4]. These coefficients can be calculated from the following equations:

$$\begin{aligned} C_{i1} &= [S'_i(S'_i+1) + S_1(S_1+1) - S_2(S_2+1)]/[2S'_i(S'_i+1)] \\ C_{i2} &= [S'_i(S'_i+1) + S_2(S_2+1) - S_1(S_1+1)]/[2S'_i(S'_i+1)] \end{aligned} \tag{5.10}$$

Table 5.1
Coefficient relating the hyperfine coupling of an S_1 or S_2 spin system in a monomer to that in a coupled system, for each S_i spin level [4]

S_1	S_2																					
	$\frac{1}{2}$			1			$\frac{3}{2}$			2			$\frac{5}{2}$			3			$\frac{7}{2}$		
	S	C_1	C_2	S	C_1	C_2	S	C_1	C_2	S	C_1	C_2	S	C_1	C_2	S	C_1	C_2	S	C_1	C_2
$\frac{1}{2}$	1	$\frac{1}{2}$	$\frac{1}{2}$	$\frac{3}{2}$	$\frac{1}{3}$	$\frac{2}{3}$	2	$\frac{1}{4}$	$\frac{3}{4}$	$\frac{5}{2}$	$\frac{1}{5}$	$\frac{4}{5}$	3	$\frac{1}{6}$	$\frac{5}{6}$	$\frac{7}{2}$	$\frac{1}{7}$	$\frac{6}{7}$	4	$\frac{1}{8}$	$\frac{7}{8}$
	0	—	—	$\frac{1}{2}$	$-\frac{1}{3}$	$\frac{4}{3}$	1	$-\frac{1}{4}$	$\frac{5}{4}$	$\frac{3}{2}$	$-\frac{1}{5}$	$\frac{6}{5}$	2	$-\frac{1}{6}$	$\frac{7}{6}$	$\frac{5}{2}$	$-\frac{1}{7}$	$\frac{8}{7}$	3	$-\frac{1}{8}$	$\frac{9}{8}$
1				2	$\frac{1}{2}$	$\frac{1}{2}$	$\frac{5}{2}$	$\frac{2}{5}$	$\frac{3}{5}$	3	$\frac{1}{3}$	$\frac{2}{3}$	$\frac{7}{2}$	$\frac{2}{7}$	$\frac{5}{7}$	4	$\frac{1}{4}$	$\frac{3}{4}$	$\frac{9}{2}$	$\frac{2}{9}$	$\frac{7}{9}$
				1	$\frac{1}{2}$	$\frac{1}{2}$	$\frac{3}{2}$	$\frac{4}{15}$	$\frac{11}{15}$	2	$\frac{1}{6}$	$\frac{5}{6}$	$\frac{5}{2}$	$\frac{4}{35}$	$\frac{31}{35}$	3	$\frac{1}{12}$	$\frac{11}{12}$	$\frac{7}{3}$	$\frac{4}{63}$	$\frac{59}{63}$
				0	—	—	$\frac{1}{2}$	$-\frac{2}{3}$	$\frac{5}{3}$	1	$-\frac{1}{2}$	$\frac{3}{2}$	$\frac{3}{2}$	$-\frac{2}{5}$	$\frac{7}{5}$	2	$-\frac{1}{3}$	$\frac{4}{3}$	$\frac{5}{2}$	$-\frac{2}{7}$	$\frac{9}{7}$
$\frac{3}{2}$							3	$\frac{1}{2}$	$\frac{1}{2}$	$\frac{7}{2}$	$\frac{3}{7}$	$\frac{4}{7}$	4	$\frac{3}{8}$	$\frac{5}{8}$	$\frac{9}{2}$	$\frac{1}{3}$	$\frac{2}{3}$	5	$\frac{3}{10}$	$\frac{7}{10}$
							2	$\frac{2}{5}$	$\frac{1}{2}$	$\frac{5}{2}$	$\frac{13}{35}$	$\frac{22}{35}$	3	$\frac{7}{24}$	$\frac{17}{24}$	$\frac{7}{2}$	$\frac{5}{21}$	$\frac{16}{21}$	4	$\frac{1}{5}$	$\frac{4}{5}$
							1	$\frac{1}{2}$	$\frac{1}{2}$	$\frac{3}{2}$	$\frac{1}{5}$	$\frac{4}{5}$	2	$\frac{1}{12}$	$\frac{11}{12}$	$\frac{5}{2}$	$\frac{1}{35}$	$\frac{34}{35}$	3	0	1
							0	—	—	$\frac{1}{2}$	-1	2	1	$-\frac{3}{4}$	$\frac{7}{4}$	$\frac{3}{2}$	$-\frac{3}{5}$	$\frac{8}{5}$	2	$-\frac{1}{2}$	$\frac{3}{2}$
2										4	$\frac{1}{2}$	$\frac{1}{2}$	$\frac{9}{2}$	$\frac{4}{9}$	$\frac{5}{9}$	5	$\frac{2}{5}$	$\frac{3}{5}$	$\frac{11}{2}$	$\frac{4}{11}$	$\frac{7}{11}$
										3	$\frac{1}{2}$	$\frac{1}{2}$	$\frac{7}{2}$	$\frac{26}{63}$	$\frac{37}{63}$	4	$\frac{7}{20}$	$\frac{13}{20}$	$\frac{9}{2}$	$\frac{10}{33}$	$\frac{23}{33}$
										2	$\frac{1}{2}$	$\frac{1}{2}$	$\frac{5}{2}$	$\frac{12}{35}$	$\frac{23}{35}$	3	$\frac{1}{4}$	$\frac{3}{4}$	$\frac{7}{2}$	$\frac{4}{21}$	$\frac{17}{21}$
										1	$\frac{1}{2}$	$\frac{1}{2}$	$\frac{3}{2}$	$\frac{2}{15}$	$\frac{13}{15}$	2	0	1	$\frac{5}{2}$	$-\frac{2}{35}$	$\frac{37}{35}$
										0	—	—	$\frac{1}{2}$	$-\frac{4}{3}$	$\frac{7}{3}$	1	-1	2	$\frac{3}{2}$	$-\frac{4}{5}$	$\frac{9}{5}$

5/2	5	1/2	1/2	11/2	5/11	6/11	6	5/12	7/12
	4	1/2	1/2	9/2	43/99	56/99	5	23/60	37/60
	3	1/2	1/2	7/2	25/63	38/63	4	13/40	27/40
	2	1/2	1/2	5/2	11/35	24/35	3	5/24	19/24
	1	1/2	1/2	3/2	1/15	14/15	2	−1/12	13/12
	0	—	—	1/2	−5/3	8/3	1	−5/4	9/4
3				6	1/2	1/2	13/2	6/13	7/13
				5	1/2	1/2	11/2	64/143	79/143
				4	1/2	1/2	9/2	14/33	19/33
				3	1/2	1/2	7/2	8/21	13/21
				2	1/2	1/2	5/2	2/7	5/7
				1	1/2	1/2	3/2	0	1
				0	—	—	1/2	−2	3
7/2							7	1/2	1/2
							6	1/2	1/2
							5	1/2	1/2
							4	1/2	1/2
							3	1/2	1/2
							2	1/2	1/2
							1	1/2	1/2
							0	—	—

Note that in the ground state of an antiferromagnetic dimer the metal 2 with smaller S_2 always has a negative coefficient, whereas metal 1 has a positive coefficient. This observation is of paramount importance to detect the establishment of antiferromagnetic coupling.

There are no treatments for the pseudocontact term, since the orbital part has never been considered when dealing with magnetic coupled systems. However, Eqs. (5.6) and (5.9) hold for the hyperfine splitting in EPR spectra of both solids and solutions [1]. Therefore the same reasoning is likely to apply to the pseudocontact shift as well. The major complication arises from the point-dipolar nature of the pseudocontact shift treatment, which contrasts with the idea of a polymetallic center.

5.2. Electron relaxation and magnetic coupling

A consequence of magnetic coupling can be a change in the electronic relaxation times of the involved metal ions. Magnetic coupling gives rise to new energy levels which can provide new relaxation pathways. New transitions involving spin levels can occur through coupling with the lattice, i.e. solvent collisions, solvent fluctuations, molecular tumbling, phonons when appropriate. This is indeed what happens in polymetallic systems. In this case there is more than one level with the same S' value which allow electronic transitions.

5.2.1. *Homodimers*

In homodimers, all the levels have different S' and in principle no further relaxation pathway is occurring. Experiments have been performed aiming at comparing the τ_s value in copper(II) dimetallic systems with respect to monometallic systems [5]. A protein frame has been used in which either only one copper(II) ion is present or two magnetically coupled copper(II) ions are present. In the latter case J is 52 cm^{-1} and all the S' levels are almost equally populated at room temperature. The protein is superoxide dismutase, whose metal ligands are shown in Fig. 5.1. We may have either copper–zinc or copper–copper systems. Nuclear longitudinal relaxation was measured for the water protons since one water molecule interacts with one copper ion. It is shown that in the two cases the copper(II) ion bound to water maintains similar τ_s values. The nuclear relaxation in the dimer is, however, one-half that in the monomer. By analogy with the shift, in dimetallic systems the relaxation rate enhancement of a nucleus sensing one metal ion is given by:

$$R_{1M} \propto E^2 S'(S'+1) f(\omega, \tau_c) \sum_i C_i^2 P_i \tag{5.11}$$

where $E^2S'(S'+1)$ is a generic notation for the average square of the interaction

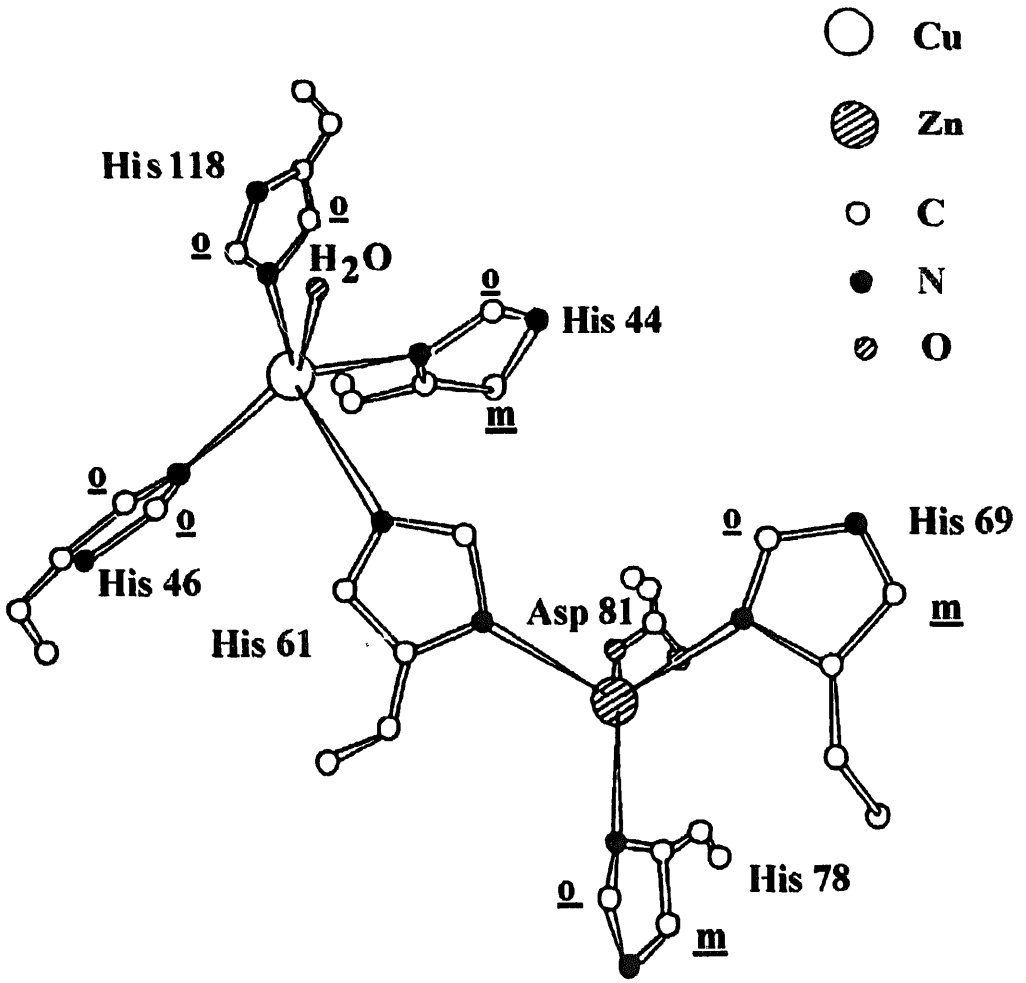

Fig. 5.1. Schematic structure of the active site of copper–zinc superoxide dismutase [6]. The zinc ion can be substituted, among others, by copper(II), cobalt(II) and nickel(II) ions.

energy between S' and I, whose modulation with time constant τ_c causes relaxation[2], $C_i = \frac{1}{2}$ for a system constituted by two ions with the same S, and P_i is the Boltzmann partition function. In the case of two $S = \frac{1}{2}$ ions and $|J| \ll kT$, $P = \frac{3}{4}$, because only the $S' = 1$ level which is threefold degenerate contributes to paramagnetic relaxation, the $S' = 0$ level being magnetically silent. Since R_{1M} for the monomer depends on $S(S+1)$ with $S = \frac{1}{2}$, and for the dimer it depends on $S'(S'+1)$ with $S' = 1$ (Eq. (5.11)), the ratio between the R_{1M} values of the dimer for a nucleus sensing only one metal ion and of the monomer is

$$\frac{C^2 S'(S'+1)P}{S(S+1)} = \frac{1/4 \times 2 \times 3/4}{3/4} = \frac{1}{2}$$

[2] $E^2 S(S+1)$ is a generic notation that holds for dipolar, contact or Curie relaxation. In the equation for Curie relaxation a term $S^2(S+1)^2$ appears, arising from the definition of $\langle S_z \rangle^2$. In the above notation, the additional $S(S+1)$ term is therefore contained in the E^2 term.

Eq. (5.11) for the case of dipolar relaxation takes the form:

$$R_{1M} = \frac{2}{15}\left(\frac{\mu_0}{4\pi}\right)^2 \frac{\gamma_I^2 g_e^2 \mu_B^2}{r^6} \times \frac{\sum_i \left[C_i^2 S_i'(S_i'+1)(2S_i'+1)\exp(-E_i/kT)\left(\frac{7\tau_c}{1+\omega_S^2\tau_c^2} + \frac{3\tau_c}{1+\omega_I^2\tau_c^2}\right)\right]}{\sum_i [(2S_i'+1)\exp(-E_i/kT)]} \tag{5.12}$$

where τ_c^{-1} is defined as usual as the sum of rotational, exchange and electronic relaxation rates. The value of τ_s, if other electronic relaxation mechanisms are not operative (see below), can be calculated [7] as a function of the transition probabilities and level lifetimes of the coupled system, and found to be close to the average between those of the isolated ions. This finding is in substantial agreement with experiments, when the factor $\frac{1}{2}$ in R_{1M} is taken into account. It is possible, however, that when there is large ZFS of the $S' = 1$ level new mechanisms of electron relaxation are effective, and τ_s shortens up. That is why sometimes the NMR linewidths of copper(II) dimers are sharper than in monomers.

Even for dimetallic centers with each metal ion having $S > \frac{1}{2}$, Eq. (5.11) provides a value of R_{1M} which is one-half of that provided by the analogous equation for the monomer. If we repeat the calculation for the hyperfine shifts (Eqs. (2.6) and (5.8)), at variance with nuclear relaxation, we see that the shifts for the coupled and uncoupled systems are the same as long as $|J| \ll kT$. Note that ferromagnetic coupling would have provided the same results because our reasoning was not based on the order of the S' levels.

When $|J|$ is of the order of kT, then the excited S' levels are not fully populated. In the case of antiferromagnetic coupling the magnetic susceptibility decreases and both shifts and nuclear relaxation values decrease. This is a significant advantage when systems with long electron relaxation times are investigated. Typically, copper(II) complexes are not easily investigated by high resolution NMR because τ_s is of the order of 10^{-9} s and τ_r for small complexes is about 10^{-10} s. Therefore, the linewidth at 500 MHz for a proton dipole–dipole coupled at 4 Å is 700 Hz in the absence of contact relaxation. In the case of a copper dimer with a J of 100 cm^{-1}, the shift of a proton sensing only one copper ion according to Eq. (5.8) is 86% of the monomeric case, and the linewidth according to Eq. (5.12) is 43% of the monomer at room temperature.

Ferromagnetic coupling generally has small $|J|$ values. For the sake of completeness, we consider the case in which there is a ferromagnetic coupling of -100 cm^{-1}. By repeating the calculations, the shifts are 111% of the monomer and the linewidths 55% of the monomer.

5.2.2. *Heterodimers*

When we deal with two different paramagnetic ions, it should be kept in mind that in the absence of magnetic coupling one will have a longer electronic relaxation

time and the other will have a shorter one, according to their electronic structure. Such differences are in general very large. The slow relaxing metal ion will be referred to as M_1 and the fast relaxing one as M_2. It is reasonable to believe that, when the absolute value of J (expressed as $|J|/\hbar$) is smaller than τ_{s1}^{-1} (i.e. the electronic relaxation rate of the slow relaxing M_1 ion) no effect on the electronic relaxation of the pair will take place. When $|J|/\hbar > \tau_{s1}^{-1}$ but smaller than τ_{s2}^{-1}, we can approach the system through a first order perturbation treatment. The coupling between S_1 and S_2 is very similar to that between I and S already discussed (Sections 3.4 and 3.5). In both cases we have a scalar coupling which is the contact coupling in the case of the electron–nucleus coupling and the exchange or superexchange coupling in the case of magnetic interactions. Analogous to the Bloembergen Eq. (3.23) for the contact nuclear relaxation we can write the following relationship:

$$\Delta\tau_{s1}^{-1} = \frac{2}{3} S_2(S_2+1)\left(\frac{J}{\hbar}\right)^2 \frac{\tau_{s2}}{1+(\omega_{S1}-\omega_{S2})^2\tau_{s2}^2} \tag{5.13}$$

where $\Delta\tau_{s1}^{-1}$ is the enhancement in the electronic relaxation rate of the slow relaxing ion, ω_{S1} and ω_{S2} are the Larmor frequencies of the M_1 and M_2 ions, and τ_{s2} is the correlation time for the interaction which is given by the electronic relaxation rate of the fast relaxing ion.

When the coupling between S_1 and S_2 is dipolar in origin the equation should again be analogous to the dipolar coupling in the case of nuclear relaxation (Eq. (3.13)):

$$\Delta\tau_{s1}^{-1} = \frac{2}{15}\left(\frac{\mu_0}{4\pi}\right)^2\left(\frac{1}{\hbar}\right)^2 \frac{g_e^4\mu_B^4 S_2(S_2+1)}{\langle r^3\rangle^2} \times \left(\frac{\tau_{s2}}{1+(\omega_{S1}-\omega_{S2})^2\tau_{s2}^2} + \frac{3\tau_{s2}}{1+\omega_{S1}^2\tau_{s2}^2} + \frac{6\tau_{s2}}{1+(\omega_{S1}+\omega_{S2})^2\tau_{s2}^2}\right) \tag{5.14}$$

where $\langle r^3\rangle$ is the average cube of the interelectronic distance.

It is apparent that the dipolar coupling is a short range coupling and rapidly vanishes with the distance. This does not hold for the scalar coupling. It is also apparent that small $|J|$ values can affect τ_{s1} under favourable conditions. In other words, small $|J|$ values can be revealed through the linewidth of the EPR signal or through NMR relaxation measurements.

Eq. (5.13) and (5.14) hold as long as $|J|/\hbar < \tau_{s2}^{-1}$. This is a general requirement in relaxation theory called Redfield limit [8]. The coupling energy between the relaxing spin and the lattice (which can be another spin) has to be smaller than the product of $\hbar$ times the reciprocal correlation time. Equivalent to this statement is the following: the relaxation rate of a spin cannot be higher than the reciprocal of the correlation time. In other words, τ_{s1}^{-1} approaches τ_{s2}^{-1} when $|J|$ increases. Outside the Redfield limit, i.e. outside the perturbative limit, each S' level should be regarded as a single spin. The transitions between $M_{S'}$ levels should be evaluated in a manner similar to that discussed for the $S > 1$ multiplets in isolated ions (Section 3.3). If reference is

made to the τ_{s1} and τ_{s2} of the single ions in the coupled system they cannot be easily predicted except for their becoming similar and close to the shorter one.

The absolute value of J, which we have used all over the treatment within the Redfield limit, implies that the theory is the same for ferro- and antiferromagnetic coupling. When $|J| \ll kT$, the sign of J is irrelevant for the nuclear shifts, the electronic relaxation times and nuclear relaxation times. When J is of the order of kT, presumably only electronic relaxation times within the various S' level can be defined, and they are independent of the sign of J, but the nuclear shifts and relaxation rates are different because the various S'_i are differently populated according to the sign of J. Eqs. (5.8) and (5.12) should be used to predict the particular behavior.

The above treatment is probably valid only in ideal cases. In practical cases spin–orbit coupling causes ZFS, and the S' levels are split at zero magnetic field just like the S levels are. This consideration requires that each S' level will have its own electronic relaxation time. The level with longest τ_s will dominate the correlation time between the nucleus and the electron. That level will have certain values of the C_i coefficients discussed earlier. Such coefficients for the level with longest τ_s should account for the observed nuclear relaxation. The drawback of the entire picture is that the τ_s values of the various S' levels are hardly predictable. Then the overall picture, as far as nuclear relaxation is concerned, should be taken as semiquantitative.

5.2.3. *Polymetallic systems*

In the case of polyionic systems the picture becomes still more complicated. There are no examples of prediction of τ_s values. However, we have empirically learned that τ_s of the entire system is shorter than in the absence of magnetic coupling. High resolution NMR experiments are, in general, successful with magnetically coupled polyionic systems.

5.3. NMR of dimetallic systems

It is convenient to divide this section into systems containing equal or different metal ions. Each of the two cases will be treated according to whether $|J|$ is larger or smaller than kT.

5.3.1. *Systems containing equal metal ions, $|J| < kT$*

We take now as an illustrative example the dimers with PMK as ligand. Such a ligand is capable of giving bimetallic complexes of formula $[(PMK)_3M_2]^{4+}$ and with the structure shown in Fig. 5.2 [9]. The ligand provides a pathway for weak magnetic coupling. When $|J| \ll kT$, the shift experienced by a nucleus is simply the sum of the contributions of the two metal ions, i.e. of two terms given by Eq. (5.8) and containing A_{M1} and C_{i1}, and A_{M2} and C_{i2} respectively. This is indeed the case, as proven by using mixed complexes with the diamagnetic zinc ion [10,11]. The correlation time for the nucleus electron coupling is given by the rotational correla-

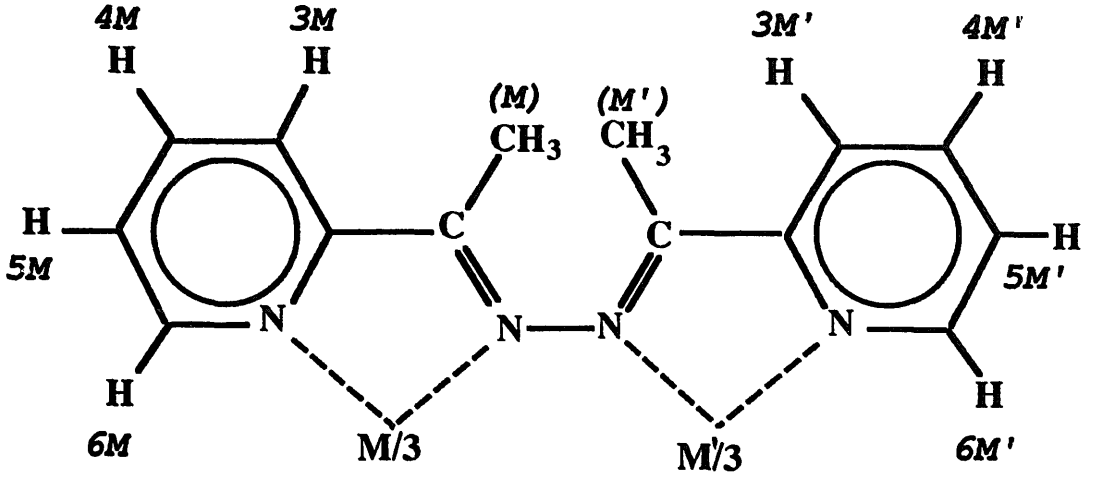

Fig. 5.2. Schematic structure of $[(PMK)_3M_2]^{4+}$ bimetallic complexes [9].

tion time in the case of copper(II) complexes ($\tau_r \approx 2 \times 10^{-10}$ s) and by the electronic relaxation time ($\tau_s \approx 6 \times 10^{-13}$ s) in the case of cobalt(II) complexes [12,13]. As explained in the previous section, a decrease is expected in the linewidth, which would be of a factor of two if the proton senses only one paramagnetic ion. Indeed, some decrease in the linewidth is observed. In Table 5.2 the NMR parameters for the CoCo system are reported, together with those of the CoZn, NiZn, CuZn, CoNi, and CoCu systems (see Section 5.3.3) [13].

5.3.2. *Systems containing equal metal ions,* $|J| \approx kT$

The first systems of this kind investigated in the literature are dicopper(II) dimers [14,15], where J is positive and of the order of hundreds of wavenumbers. The correlation time is τ_r; the nuclear relaxation rates, as well as the shifts, are decreased according to the Boltzmann partition coefficients of Eqs. (5.12) and (5.8) respectively. A factor larger than two in nuclear relaxation rate between coupled and uncoupled systems should be operative if only one metal ion is sensed by the resonating nucleus. The decrease in magnetic susceptibility due to the population of the lower part of the energy ladder makes these systems more suitable for NMR investigation than the uncoupled ones. The same holds for μ-oxo iron(III) dimers [16].

In Fig. 5.3 the spectra of a copper(II) dimer are shown [15]. The temperature dependence of the shifts is consistent, according to Eq. (5.8), with a J value of about 500 cm^{-1}. In the inset, the ^2H NMR spectrum of a selectively deuterated derivative is reported [15], showing the smaller linewidth of the ^2H signal.

When the dimetallic center is embedded in a protein, the correlation time is given by the electronic relaxation time. A studied case is provided by the $[Fe_2S_2]^{2+}$ unit represented in Fig. 5.4 and found in oxidized ferredoxins. The large correlation time makes the system difficult to investigate by NMR [17,18] despite the sizable decrease in paramagnetism due to a J of about 300 cm^{-1}.

Table 5.2
Proton hyperfine shifts (ppm) and T_{1M}^{-1} values (s^{-1}, estimated errors in parentheses) for $MM'(PMK)_3^{4+}$ complexes [13]

		3-H	4-H	5-H	6-H	$-CH_3$
CoZn(PMK)$_3^{4+}$						
Shifts	(Co)	66.81	2.74	42.31	141.47	44.99
	(Zn)	−9.88	2.41	−10	−0.69[a]	8.08
T_{1M}^{-1}	(Co)	36.1 (0.9)	11.5 (0.3)	29.2 (0.7)	670 (220)	71.9 (1.6)
	(Zn)	6.9 (0.3)	1.41 (0.02)	1.78 (0.06)	3.97 (0.06)[a]	37.3 (0.6)
NiZn(PMK)$_3^{4+}$						
Shifts	(Ni)	62.98	8.54	40.29		39.23
	(Zn)	−9.15	2.76	−8.07	2.11	−10.51
T_{1M}^{-1}	(Ni)	2000 (500)	590 (5)	1630 (110)		5900 (350)
	(Zn)	370 (15)	120 (10)	140 (10)	310 (15)	2600
CuZn(PMK)$_3^{4+}$						
Shifts	(Cu)	39.68	5.68	23.43		17.26
	(Zn)	−4.19	1.31	−3.67	0.87	−3.55
T_{1M}^{-1}	(Cu)		235 (3)	526 (60)		1200 (40)
	(Zn)	118 (10)	43.3 (1)	64 (6)	121 (2)	709 (10)
Co$_2$*(PMK)*$_3^{4+}$						
Shifts		56.46	5.08	31.99	141.21	51.88
T_{1M}^{-1}		48.5 (0.5)	17.0 (0.1)	35.8 (0.3)	588 (35)	114 (2)
CoNi(PMK)$_3^{4+}$						
Shifts	(Co)	56.54	4.74	34.47	140.55	33.75
	(Ni)	50.75	11.05	28.91	148.8[b]	44.65
T_{1M}^{-1}	(Co)	52.1 (1.4)	18.6 (0.2)	38.0 (0.6)	645 (17)	180 (0.4)
	(Ni)	112 (3)	35.2 (0.5)	88.5 (1.6)	909 (83)[b]	225 (7)
CoCu(PMK)$_3^{4+}$						
Shifts	(Co)	62.43	3.78	38.61	143.84	41.35
	(Cu)	27.60	8.06	12.21	87.38	24.65
T_{1M}^{-1}	(Co)	40.8 (1.8)	13.5 (0.4)	30.3 (1.2)	529 (28)	94.3 (3.6)
	(Cu)	37.7 (1.8)	8.33 (0.14)	24.2 (0.4)	307 (10)	75.8 (2.3)

[a] Direct overlap with 5-H (Zn_2). [b] Broad and overlapping with the other 6-H signal.

5.3.3. *Systems containing different metal ions, $|J| < kT$*

With the PMK ligand a CoCu derivative has been obtained [8] (Fig. 5.5). From the temperature dependence of the shifts (and magnetic susceptibility measurements in solution), the value of J appears to be positive and much smaller than kT [13]. As expected, the hyperfine shifts are the sum of those of the CuZn and ZnCo systems for each proton (Table 5.2). The NMR lines of the copper domain are now quite sharp, even sharper than those of the cobalt domain (Fig. 5.5). Qualitatively, the data can be accounted for if τ_s of copper is sizably reduced and approaches that of cobalt. The magnetic coupling is antiferromagnetic with an $S' = 1$ ground state and an $S' = 2$ excited state. The C_i coefficients are those of Table 5.1, i.e. $-\frac{1}{4}$ and $\frac{1}{4}$ for

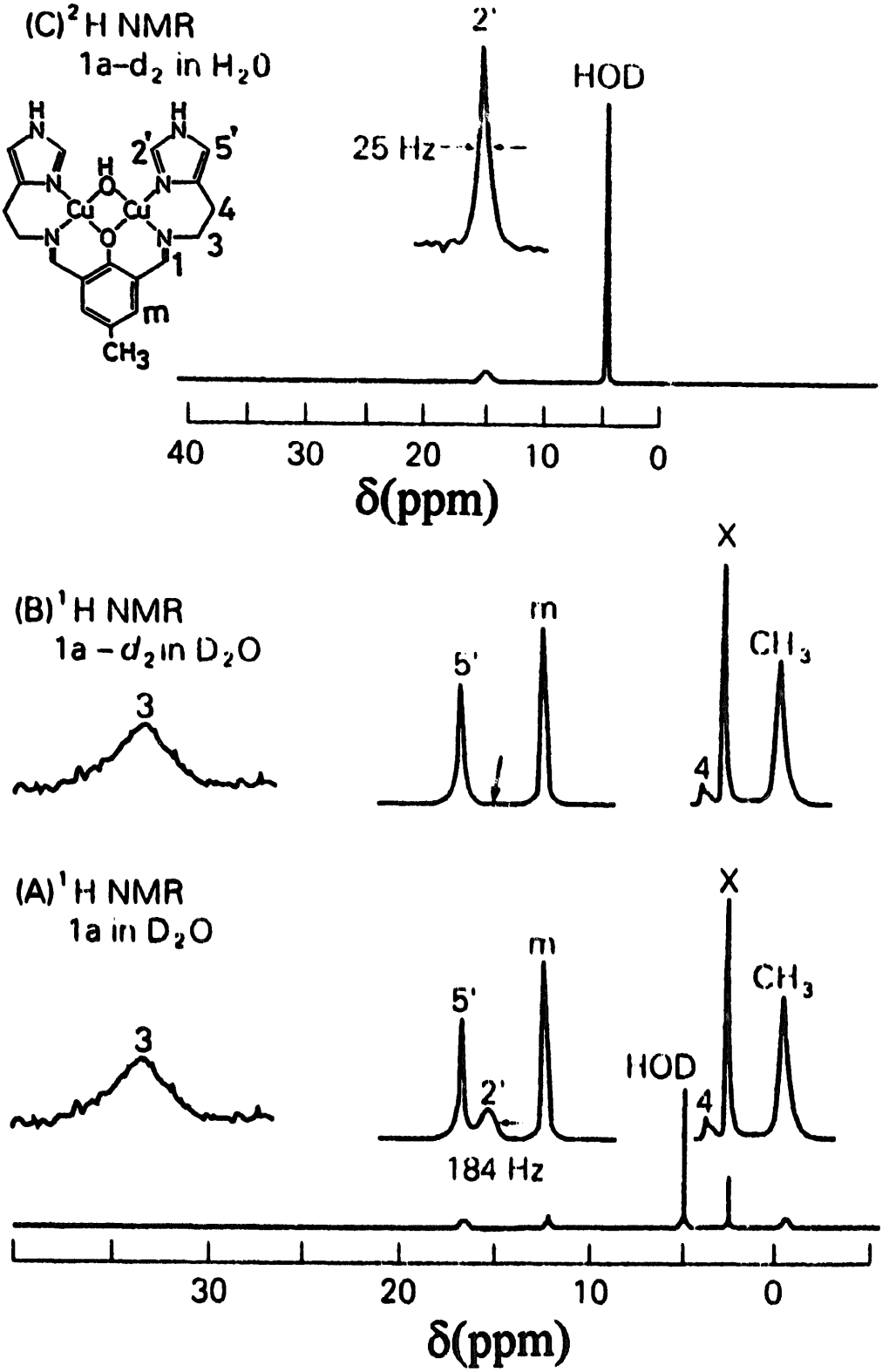

Fig. 5.3. ^{1}H NMR spectra of a copper(II) dimer (A) and of its selectively deuterated derivative (B) (the arrow pointing to the missing signal). The ^{2}H NMR spectrum of the latter is shown in (C), together with the structure of the compound [15].

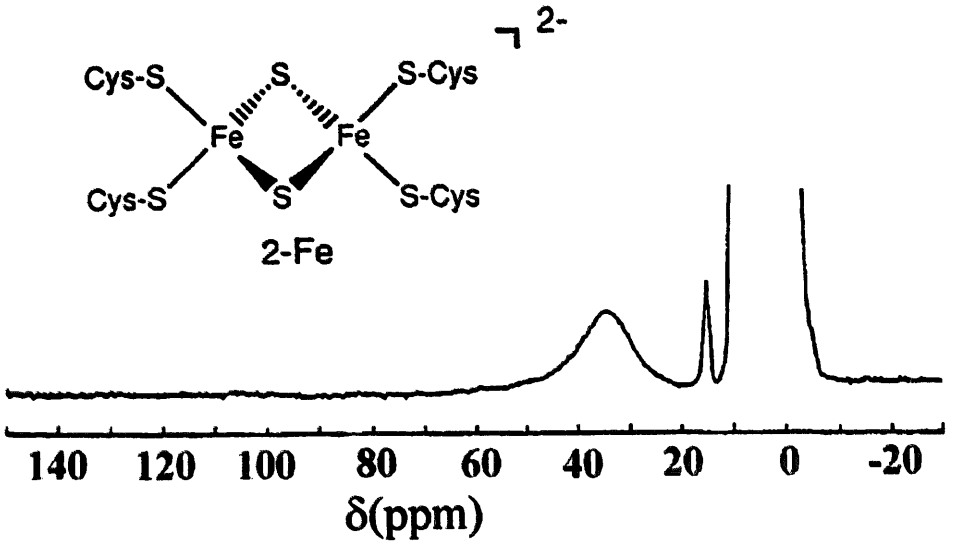

Fig. 5.4. Schematic structure of the $[Fe_2S_2](SR)_4^{2-}$ unit as found in oxidized ferredoxins and ^1H NMR spectrum showing the β-CH_2 proton signals at about 40 ppm.

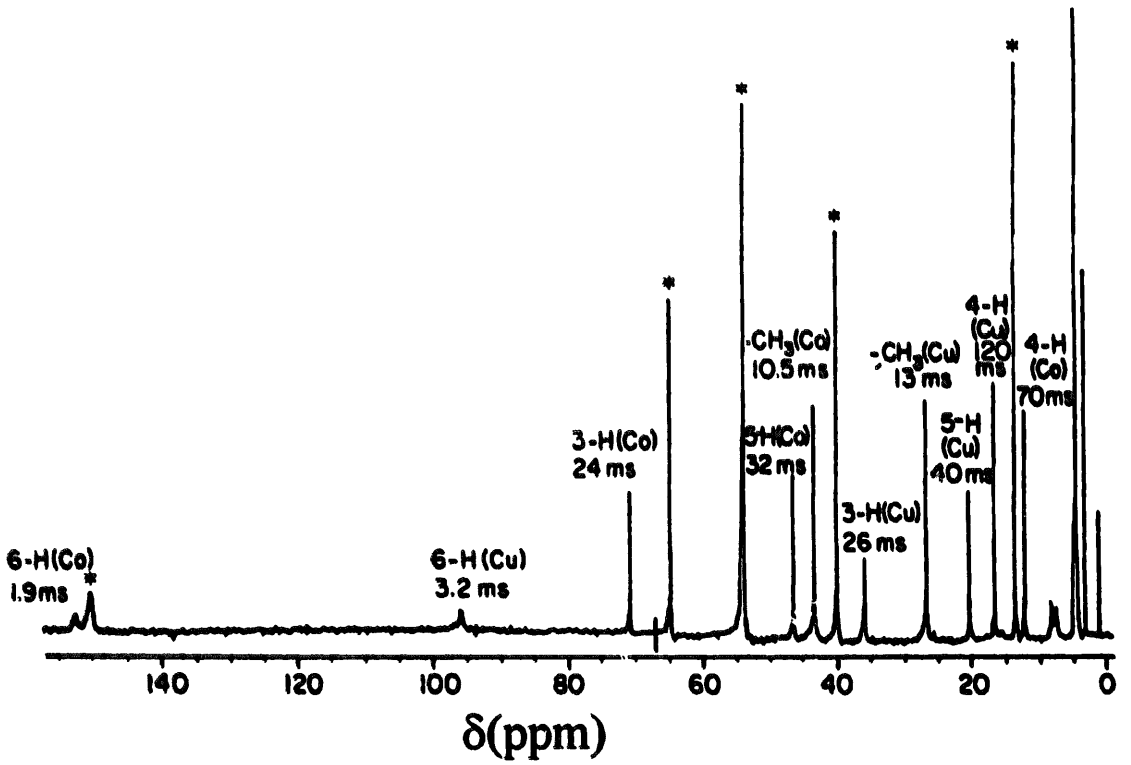

Fig. 5.5. ^1H NMR spectra of the CoCu derivative of PMK (Fig. 5.2) [13].

copper and $\frac{5}{4}$ and $\frac{3}{4}$ for cobalt. Such coefficients provide a ratio in nuclear R_{1M} of ca. 12 for the protons of the cobalt domain with respect to those of the copper domain, if τ_s were the same (Eq. (5.12)). The experimental ratio is about two. The discrepancy can be understood by considering: (i) that the electronic relaxation times

for the two metal ions are not identical; (ii) copper(II) tends to give rise to ligand-centered effects more than cobalt, and therefore to experience higher nuclear relaxation rates than expected on the basis of a pure dipolar mechanism; (iii) the presence of ZFS complicates the prediction strategies.

The above system is similar to that built into the protein superoxide dismutase. The protein is a dimer of $MW \approx 32000$, each subunit containing a copper–zinc moiety as shown in Fig. 5.2. The zinc can be replaced by several metal ions. Cobalt(II) and nickel(II) are pertinent here. The cobalt–copper system has $J \approx 17\ cm^{-1}$ with $S' = 1$ ground state [19]. The electronic relaxation times for the two ions are expected to be either equal or similar. The ^1H NMR spectrum is shown in Fig. 5.6(A). The assignment has been performed through several steps:

(a) the histidine NH protons have been recognized because their signals disappear when the spectrum is recorded in D_2O (Fig. 5.6(A)) [22];

(b) the protons of the copper domain have smaller R_1 than those of the cobalt domain if the metal–proton distances are similar [22];

(c) the linewidths have large Curie relaxation contributions which can be factorized out by recording the spectra at different fields. Such contributions and the R_1 values should provide a qualitative order of distances of the protons from the metal ions. However, large spin delocalization effects may provide larger linewidths to protons farther from the metal ion and this has lead to a misassignment [23];

(d) NOE measurements have allowed the assignment of all histidine protons and of the β-CH_2 of the Asp group [20];

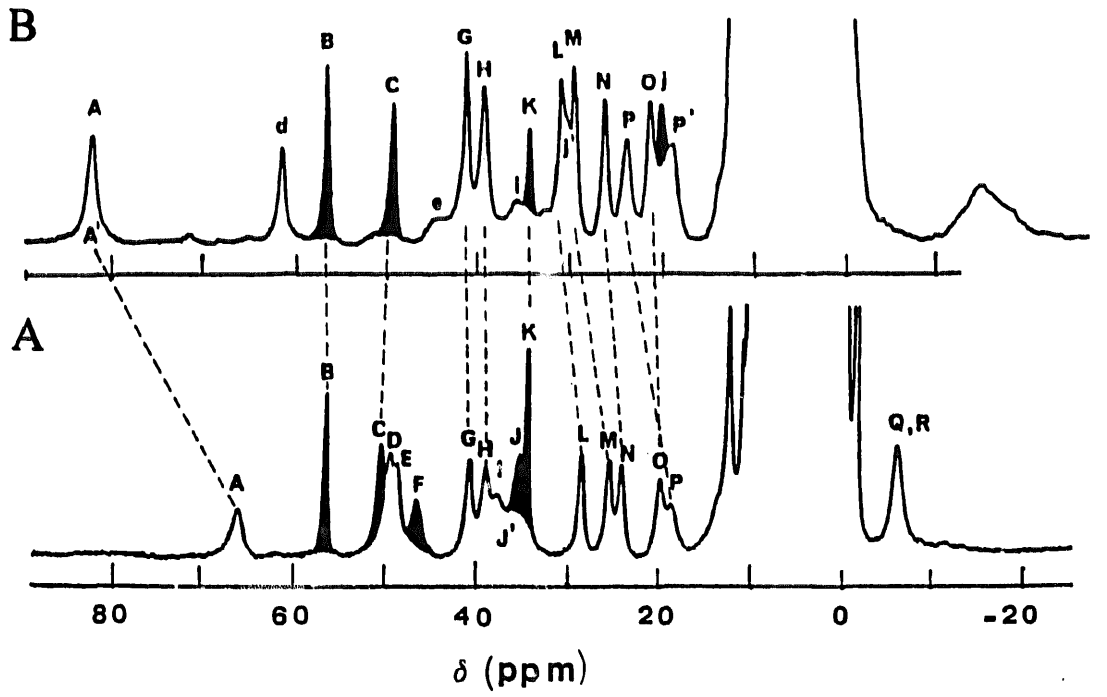

Fig. 5.6. ^1H NMR spectra of Cu_2Co_2 (A) [20] and Cu_2Ni_2 (B) [21] superoxide dismutase. The dashed lines relate signals belonging to the various histidine ligands of the copper domain. The black-shaded signals disappear when the spectra are recorded in D_2O.

(e) NOESY spectra have largely confirmed the previous assignment and have permitted the assignment of the β-CH_2 protons and of some α-CH protons of the histidines [20].

The resulting assignment, which is one of the most successful in paramagnetic metalloproteins, is reported in Table 5.3. The nuclear relaxation rates, which are in a ratio similar to those of the CuCoPMK system, have been interpreted on the basis of large ligand-centered effects on the copper ligands [20].

The value of J is not known in the case of the copper–nickel derivative. However, the same line of discussion should hold for this derivative, whose spectrum is shown in Fig. 5.6(B) [21]. It is noteworthy that the R_1 values of the protons of the copper domain are smaller in this case than in the cobalt case. This is probably due to a shorter electronic relaxation time of tetrahedral nickel(II) than tetrahedral cobalt(II) (see Section 3.3). In this respect it may be interesting to note that in the case of the cobalt–cobalt derivative we have a tetrahedral and a square pyramidal cobalt(II) ion [24]. The former has longer electronic relaxation times. Upon establishment of magnetic coupling, the electronic relaxation times of the tetrahedral cobalt(II) ion decrease and tend to reach the values of the square pyramidal cobalt(II) ion. This is evident by comparing the spectra of the protein containing only the tetrahedral cobalt(II) ion with those containing both ions (Fig. 5.7).

Many systems of this kind are available in the literature. Only a small part has been studied by NMR, and sometimes not all the structural and dynamic information has been extracted from the spectra with the support of the available theory.

The results are expected to be the same if the coupling is of ferromagnetic type.

5.3.4. *Systems containing different metal ions, $|J| \approx kT$*

If $|J|$ were much larger than kT, only the ground state would be populated. This limit condition is very useful to illustrate the peculiarities of asymmetric dimeric systems. In these systems, one ion will have a spin larger than the other. In the ground state the larger spin will always be aligned along the external magnetic field. Now we can distinguish between ferro- and antiferromagnetic coupling. In the former case the smaller spin is aligned along with the larger spin; in the latter case the smaller spin is forced to be aligned opposite to the external magnetic field. The second case is the most common. The larger spin provides a "normal" additional magnetic field to the resonating nucleus in a way similar to the case of absence of magnetic coupling. The smaller spin is forced to provide an additional field of different sign. From the theory we do expect a negative sign for the coefficient related to the smaller spin (see Eqs. (5.9) and (5.10)). Therefore, if the nuclei coupled to the larger spin experience downfield shift, the nuclei coupled to the smaller spin will experience upfield shifts (Fig. 5.8). In the limit of $|J| \ll kT$ the shifts of the two kinds of nuclei are the same as if there were no magnetic coupling at all. In the intermediate cases the shifts of the nuclei coupled to the smaller spin can be anywhere from downfield to upfield. However, if they are downfield, they will increase with increasing temperature, as the system will tend towards $|J| \ll kT$. The shifts of the nuclei coupled to the larger spin will decrease with increasing temperature similarly to a normal

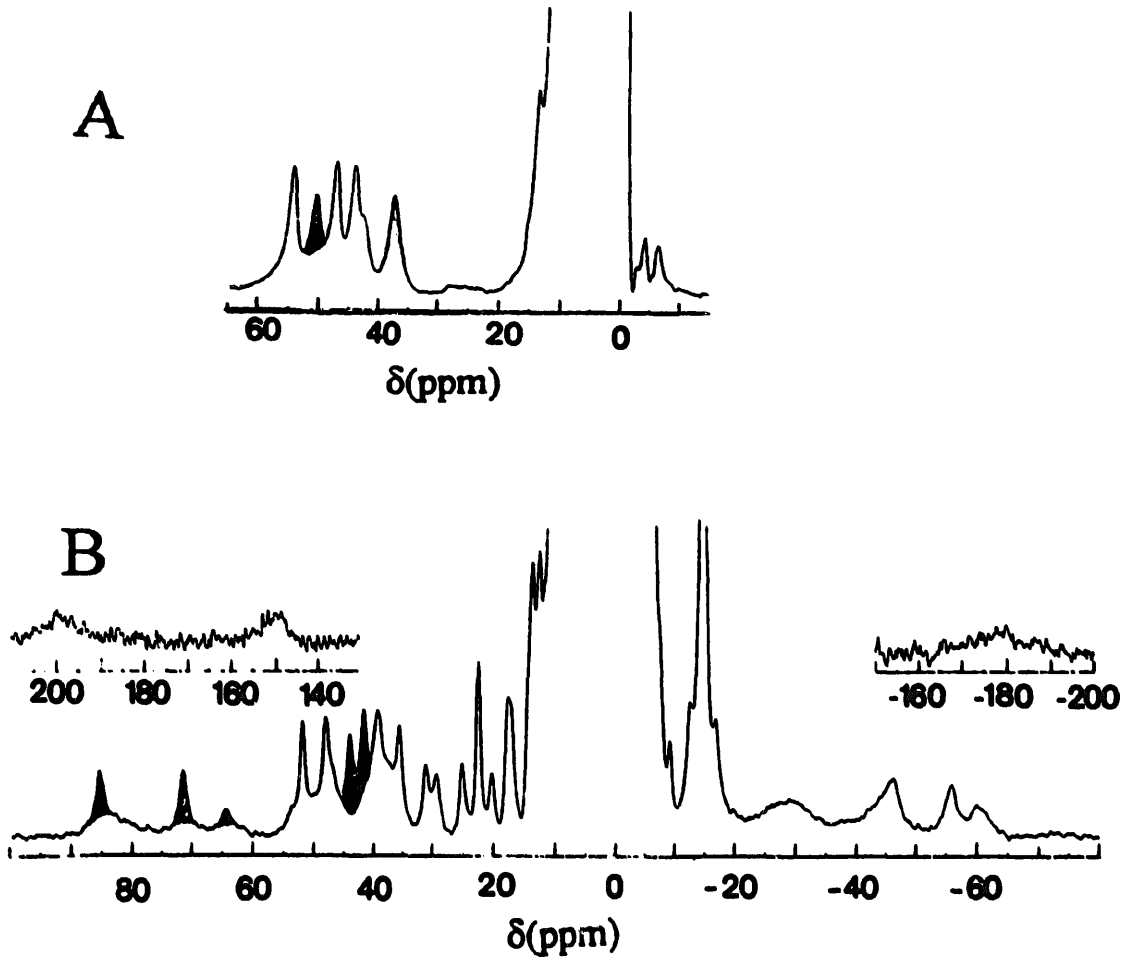

Fig. 5.7. ^{1}H NMR spectra of E_2Co_2 (A) (E = empty) and Co_2Co_2 superoxide dismutase (B). The black-shaded signals disappear when the spectra are recorded in D_2O [24].

paramagnet (see Eqs. (2.5) and (2.6)). The expected temperature dependence is illustrated in Fig. 5.9, as calculated from Eq. (5.8).

From the point of view of relaxation we expect similar values of τ_s for the two spins, unless ZFS of the magnetically coupled S' levels introduces unpredictable effects.

The best case studied is that of reduced $[Fe_2S_2]^+$-containing ferredoxins [25,26]. The systems contain one iron(III) and one iron(II) ions (Fig. 5.10 inset). Both of them are tetrahedral and high spin. The iron(III) has $S = \frac{5}{2}$ and the iron(II) $S = 2$. The ^{1}H NMR spectrum of one protein is reported in Fig. 5.10 [25]. The four signals far downfield belong to the β-CH_2 protons of the two cysteines bound to iron(III). Such signals have a temperature dependence of Curie type, i.e. the hyperfine shifts increase with decreasing temperature. The sharp signal around 40 ppm is assigned to an α-CH proton of one cysteine of the iron(III) domain. The four sharp signals between 30 and 15 ppm belong to the β-CH_2 protons of the cysteines of the iron(II)

Table 5.3
Assignment of ^1H NMR signals of metal coordinated residues in Cu_2Co_2SOD (298 K, pH 5.5, buffer 50 mM acetate). The tentative assignment of some signals involving residues not directly bound to the metal ions, and falling in the diamagnetic region of Fig. 5.6(A) is also reported [20]

Signal	Shift (ppm)	Assignment
A	67.4	His 63 $H\delta_2$
B	57.0	His 120 $HN\delta_1$
C	50.3	His 46 $HN\varepsilon_2$
D	49.6	His 71 $H\delta_2$
E	49.0	His 80 $H\delta_2$
F	46.7	His 80 $HN\varepsilon_2$
G	41.0	His 46 $H\delta_2$
H	39.5	His 120 $H\varepsilon_1$
I	38.7	Asp 83 $H\beta_1$
J'	37.0	Asp 83 $H\beta_2$
J	35.6	His 71 $HN\varepsilon_2$
K	34.7	His 48 $HN\delta_1$
L	28.4	His 48 $H\delta_2$
M	25.7	His 46 $H\varepsilon_1$
N	24.3	His 120 $H\delta_2$
O	19.8	His 48 $H\varepsilon_1$
P	18.7	His 46 $H\beta_1$
Q	−6.2	His 71 $H\beta_2$
R	−6.2	His 46 $H\beta_2$
a'	12.30	His 48 $H\beta_2$
b'	11.21	His 120 $H\beta_2$
c'	8.44	His 120 NH
d'	6.40	His 48 $H\beta_1$
e'	4.43	His 120 $H\alpha$
f'	3.73	His 48 $H\alpha$
g'	3.13	His 120 $H\beta_1$
h'	1.23	Ala 140 βCH_3
i'	0.56	Val 118 $\gamma_1 CH_3$
j'	−0.28	Arg 143 $H\gamma_1$
k'	−1.51	Val 118 $\gamma_1 CH_3$

domain. The latter four signals have a temperature dependence of antiCurie type, i.e. the hyperfine shifts increase with increasing temperature.

NOE studies have shown the pairwise nature of the β-CH_2 protons of the cysteines of the iron(II) domain [27]; the β-CH_2 proton signals of the iron(III) domain are too broad to observe any dipolar connectivity. Inter-β-CH_2 NOEs have also been observed between two signals of two β-CH_2 of the iron(II) domain, thus providing a key information to assign the cysteines bound to iron(II) to Cys-41 and Cys-46 and, by exclusion, the cysteines bound to iron(III) to Cys-49 and Cys-79. In fact, by analyzing the X-ray structure it appears that Cys-41 and Cys-46 are close enough

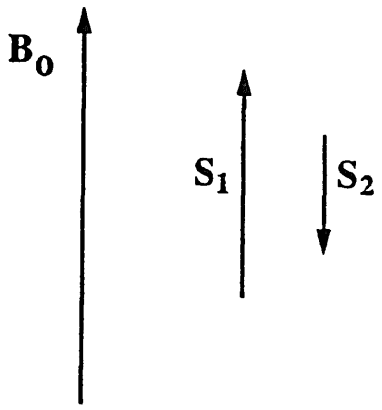

Fig. 5.8. Pictorial scheme of the magnetic moments corresponding to S_1 and S_2 induced by a magnetic field B_0 in an antiferromagnetically coupled ground state, S_1 being larger than S_2, and $g_e\mu_B B_0 \ll J$.

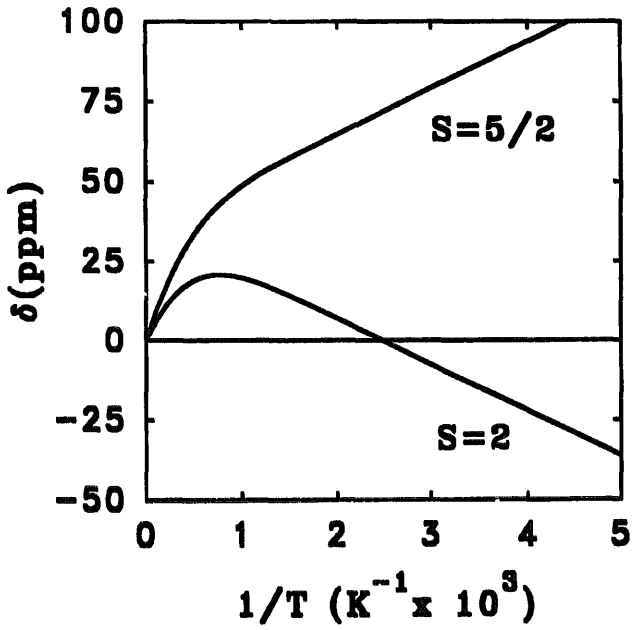

Fig. 5.9. Predicted temperature dependence of the shifts of nuclei sensing either the $S = \frac{5}{2}$ or the $S = 2$ spin of an antiferromagnetically coupled pair with $J = 300\ \mathrm{cm}^{-1}$.

to one another to give inter-residue NOE. The detection of the iron(III) and iron(II) domains is a piece of information that only NMR could have provided.

5.4. Polymetallic systems

In polymetallic systems, the larger the number of coupled ions, the larger the spreading of the S' levels. As a consequence, even relatively small $|J|$ values give rise

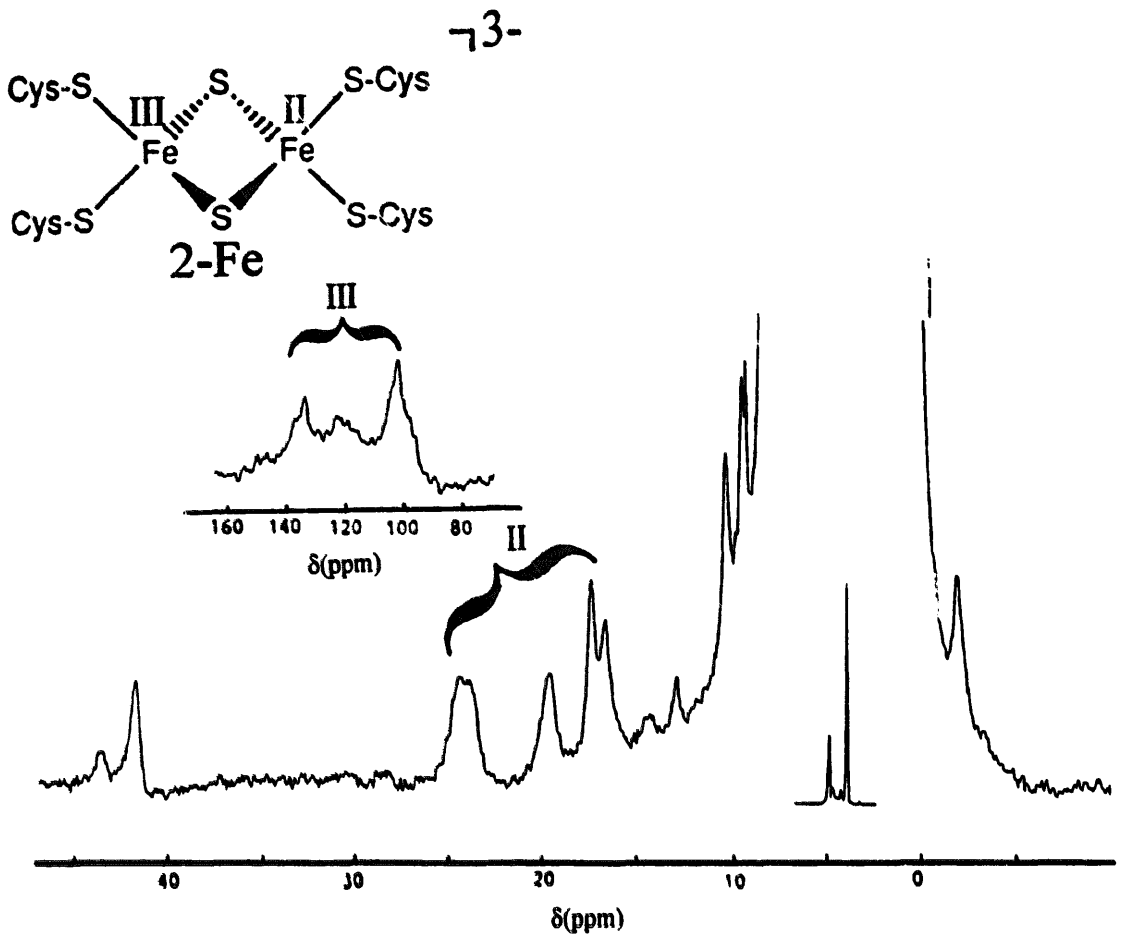

Fig. 5.10. ^{1}H NMR spectra of reduced Fe_2S_2 ferredoxin containing one iron(II) and one iron(III) ions antiferromagnetically coupled. The roman number labeling II and III refers to the oxidation states of the iron ions to which the cysteines are bound [25].

to large separations of the S' levels and therefore to depopulation of the highest levels. The general theory is still the same. Analytical solutions, as in dimeric systems, are seldom possible. Often, only numerical solutions are possible.

The general Hamiltonian is given by Eq. (5.3), where the sum is over all the j–k pairs. The treatment is in fact based on bimetallic coupling. The S' levels are obtained and the hyperfine coupling for each S' level is given by

$$A_{ij} = A_j \frac{\langle S_{jz} \rangle_i}{\langle S'_z \rangle_i} = A_j C_{ij} \tag{5.15}$$

where A_{ij} is the hyperfine coupling between the ith S' level and a nucleus sensing the jth metal. A_j is the hyperfine coupling between the nucleus and the spin on the jth metal (S_j) in the absence of magnetic coupling. $\langle S_{jz} \rangle_i$ is the contribution of metal j (S_j) to the expectation value of S'_z of the ith level. This equation is quite analogous to Eq. (5.6).

Under certain symmetry conditions, Eq. (5.3) can be rearranged in order to allow for analytical solutions[3]. In trimetallic systems, when $J_{12} \neq J_{13} = J_{23}$, Eq. (5.3) becomes [1]

$$\mathscr{H} = J(\boldsymbol{S}_1 \cdot \boldsymbol{S}_2 + \boldsymbol{S}_1 \cdot \boldsymbol{S}_3 + \boldsymbol{S}_2 \cdot \boldsymbol{S}_3) + \Delta J_{12} \boldsymbol{S}_1 \cdot \boldsymbol{S}_2 \tag{5.16}$$

where ΔJ_{12} indicates the difference between J_{12} and the other two J values. The energies are

$$E(S'_{12}, S') = \frac{1}{2}[JS'(S'+1) + \Delta J_{12} S'_{12}(S'_{12}+1)] \tag{5.17}$$

where S'_{12} is the subspin value coming out from the coupling of spins 1 and 2.

The coefficients C_{ij} in Eq. (5.15) are then given by [28]

$$\begin{aligned} C_{i1} &= [S'(S'+1) + S'_{12}(S'_{12}+1) - S_3(S_3+1)]/2S'(S'+1) \\ &\quad \times [S'_{12}(S'_{12}+1) + S_1(S_1+1) - S_2(S_2+1)]/2S'_{12}(S'_{12}+1) \\ C_{i2} &= [S'(S'+1) + S'_{12}(S'_{12}+1) - S_3(S_3+1)]/2S'(S'+1) \\ &\quad \times [S'_{12}(S'_{12}+1) + S_2(S_2+1) - S_1(S_1+1)]/2S'_{12}(S'_{12}+1) \\ C_{i3} &= [S'(S'+1) + S_3(S_3+1) - S'_{12}(S'_{12}+1)]/2S'(S'+1) \end{aligned} \tag{5.18}$$

For tetraionic systems, analytical solutions are possible in the two following cases [29–31]:

(a) $J_{12} \neq J_{34} \neq J_{13} = J_{14} = J_{23} = J_{24}$

$$\begin{aligned} \mathscr{H} &= J(\boldsymbol{S}_1 \cdot \boldsymbol{S}_2 + \boldsymbol{S}_1 \cdot \boldsymbol{S}_3 + \boldsymbol{S}_1 \cdot \boldsymbol{S}_4 + \boldsymbol{S}_2 \cdot \boldsymbol{S}_3 + \boldsymbol{S}_2 \cdot \boldsymbol{S}_4 + \boldsymbol{S}_3 \cdot \boldsymbol{S}_4) \\ &\quad + \Delta J_{12}(\boldsymbol{S}_1 \cdot \boldsymbol{S}_2) + \Delta J_{34}(\boldsymbol{S}_3 \cdot \boldsymbol{S}_4) \end{aligned} \tag{5.19}$$

$$E(S'_{12}, S'_{34} S') = \frac{1}{2}[JS'(S'+1) + \Delta J_{12} S'_{12}(S'_{12}+1) + \Delta J_{34} S'_{34}(S'_{34}+1)] \tag{5.20}$$

---

[3] In case all J values are equal, the eigenvalues of the Hamiltonian $\mathscr{H} = J(\boldsymbol{S}_1 \cdot \boldsymbol{S}_2 + \boldsymbol{S}_1 \cdot \boldsymbol{S}_3 + \boldsymbol{S}_2 \cdot \boldsymbol{S}_3)$ can be obtained by trivial extension of the dimer case. As $\boldsymbol{S}' = \boldsymbol{S}_1 + \boldsymbol{S}_2 + \boldsymbol{S}_3$, we can square the total $\boldsymbol{S}'$ value to obtain: $S'^2 = S_1^2 + S_2^2 + S_3^2 + 2\boldsymbol{S}_1 \cdot \boldsymbol{S}_2 + 2\boldsymbol{S}_1 \cdot \boldsymbol{S}_3 + 2\boldsymbol{S}_2 \cdot \boldsymbol{S}_3$, and write: $\mathscr{H} = (J/2)(S'^2 - S_1^2 - S_2^2 - S_3^2)$, whose eigenvalues are: $E = (J/2)[S'(S'+1) - S_1(S_1+1) - S_2(S_2+1) - S_3(S_3+1)]$. Since $S_1(S_1+1)$, $S_2(S_2+1)$ and $S_3(S_3+1)$ are the same for all levels, they introduce only an energy offset and can be dropped. The splitting of the levels is just given by: $E = (J/2)S'(S'+1)$.

Analytical solutions can still be obtained when one J value (e.g. J_{12}) differs from the other two. From Hamiltonian (5.16), $\mathscr{H} = J(\boldsymbol{S}_1 \cdot \boldsymbol{S}_2 + \boldsymbol{S}_1 \cdot \boldsymbol{S}_3 + \boldsymbol{S}_2 \cdot \boldsymbol{S}_3) + \Delta J_{12} \boldsymbol{S}_1 \cdot \boldsymbol{S}_2$. We can define a subspin $\boldsymbol{S}'_{12}$ such that $\boldsymbol{S}'_{12} = \boldsymbol{S}_1 + \boldsymbol{S}_2$ and, from its square, $\boldsymbol{S}_1 \cdot \boldsymbol{S}_2 = \frac{1}{2}(S'^2_{12} - S_1^2 - S_2^2)$. Then, from the previous definitions, $\mathscr{H} = (J/2)(S'^2 - S_1^2 - S_2^2 - S_3^2) + (\Delta J_{12}/2)(S'^2_{12} - S_1^2 - S_2^2)$. Dropping again the constant terms, the eigenvalues are: $E = (\frac{1}{2})[JS'(S'+1) + \Delta J_{12} S'_{12}(S'_{12}+1)]$ (Eq. (5.17)).

$$C_{i1} = [S'(S'+1) + S'_{12}(S'_{12}+1) - S'_{34}(S'_{34}+1)]/2S'(S'+1)$$
$$\times [S'_{12}(S_{12}+1) + S_1(S_1+1) - S_2(S_2+1)]/2S'_{12}(S'_{12}+1)$$
$$C_{i2} = [S'(S'+1) + S'_{12}(S'_{12}+1) - S'_{34}(S'_{34}+1)]/2S'(S'+1)$$
$$\times [S'_{12}(S'_{12}+1) + S_2(S_2+1) - S_1(S_1+1)]/2S'_{12}(S'_{12}+1)$$
$$C_{i3} = [S'(S'+1) + S'_{34}(S'_{34}+1) - S'_{12}(S'_{12}+1)]/2S'(S'+1)$$
$$\times [S'_{34}(S'_{34}+1) + S_3(S_3+1) - S_4(S_4+1)]/2S'_{34}(S'_{34}+1)$$
$$C_{i4} = [S'(S'+1) + S'_{34}(S'_{34}+1) - S'_{12}(S'_{12}+1)]/2S'(S'+1)$$
$$\times [S'_{34}(S'_{34}+1) + S_4(S_4+1) - S_3(S_3+1)]/2S'_{34}(S'_{34}+1) \quad (5.21)$$

Here S'_{12}, S'_{34} and S' are good quantum numbers for the relative subspins.

(b) $J_{12} \neq J_{13} = J_{23} \neq J_{14} = J_{24} = J_{34}$

$$\mathcal{H} = J(\boldsymbol{S}_1 \cdot \boldsymbol{S}_2 + \boldsymbol{S}_1 \cdot \boldsymbol{S}_3 + \boldsymbol{S}_1 \cdot \boldsymbol{S}_4 + \boldsymbol{S}_2 \cdot \boldsymbol{S}_3 + \boldsymbol{S}_2 \cdot \boldsymbol{S}_4 + \boldsymbol{S}_3 \cdot \boldsymbol{S}_4)$$
$$+ \Delta J_{12}(\boldsymbol{S}_1 \cdot \boldsymbol{S}_2) + \Delta J_{123}(\boldsymbol{S}'_{12} \cdot \boldsymbol{S}_3) \quad (5.22)$$

$$E(S'_{12}, S'_{123}, S') = \frac{1}{2}[JS'(S'+1) + \Delta J_{12}S'_{12}(S'_{12}+1) + \Delta J_{123}S'_{123}(S'_{123}+1)] \quad (5.23)$$

$$C_{i1} = [S'(S'+1) + S'_{123}(S'_{123}+1) - S_4(S_4+1)]/2S'(S'+1)$$
$$\times [S'_{123}(S'_{123}+1) + S'_{12}(S'_{12}+1) - S_3(S_3+1)]/2S'_{123}(S'_{123}+1)$$
$$\times [S'_{12}(S'_{12}+1) + S_1(S_1+1) - S_2(S_2+1)]/2S'_{12}(S'_{12}+1)$$
$$C_{i2} = [S'(S'+1) + S'_{123}(S'_{123}+1) - S_4(S_4+1)]/2S'(S'+1)$$
$$\times [S'_{123}(S'_{123}+1) + S'_{12}(S'_{12}+1) - S_3(S_3+1)]/2S'_{123}(S'_{123}+1)$$
$$\times [S'_{12}(S'_{12}+1) + S_2(S_2+1) - S_1(S_1+1)]/2S'_{12}(S'_{12}+1)$$
$$C_{i3} = 1 - C_{i1} - C_{i2} - C_{i4}$$
$$C_{i4} = [S'(S'+1) + S_4(S_4+1) - S'_{123}(S'_{123}+1)]/2S'(S'+1) \quad (5.24)$$

Here ΔJ_{12} indicates the difference between J_{12} and J, ΔJ_{123} the difference between J_{13} ($= J_{23}$) and J, and S'_{123} the subspin resulting from the coupling of S'_{12} and S_3.

All of these cases have been analyzed in NMR studies [4,32].

When the same metals differ in the oxidation states, i.e. Fe^{3+} and Fe^{2+}, the treatment may be even more complicated [29–34]. We will deal with these systems later.

5.4.1. *The $[(RS)_3Fe_3S_4]^{2-}$ case*

In this case there are three $S = \frac{5}{2}$ Fe^{3+} ions antiferromagnetically coupled [28]. One J value (e.g. J_{12}) is larger than the other two (Fig. 5.11). It follows that S'_{12}

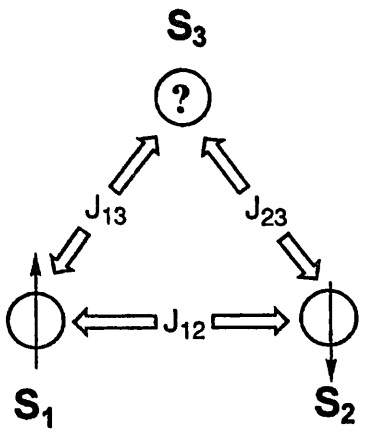

Fig. 5.11. Magnetic coupling scheme in an Fe_3 system. If $J_{12} > J_{13}, J_{23}$, S_1 and S_2 are antiferromagnetically coupled, and S_3 cannot be antiferromagnetically coupled to both S_1 and S_2.

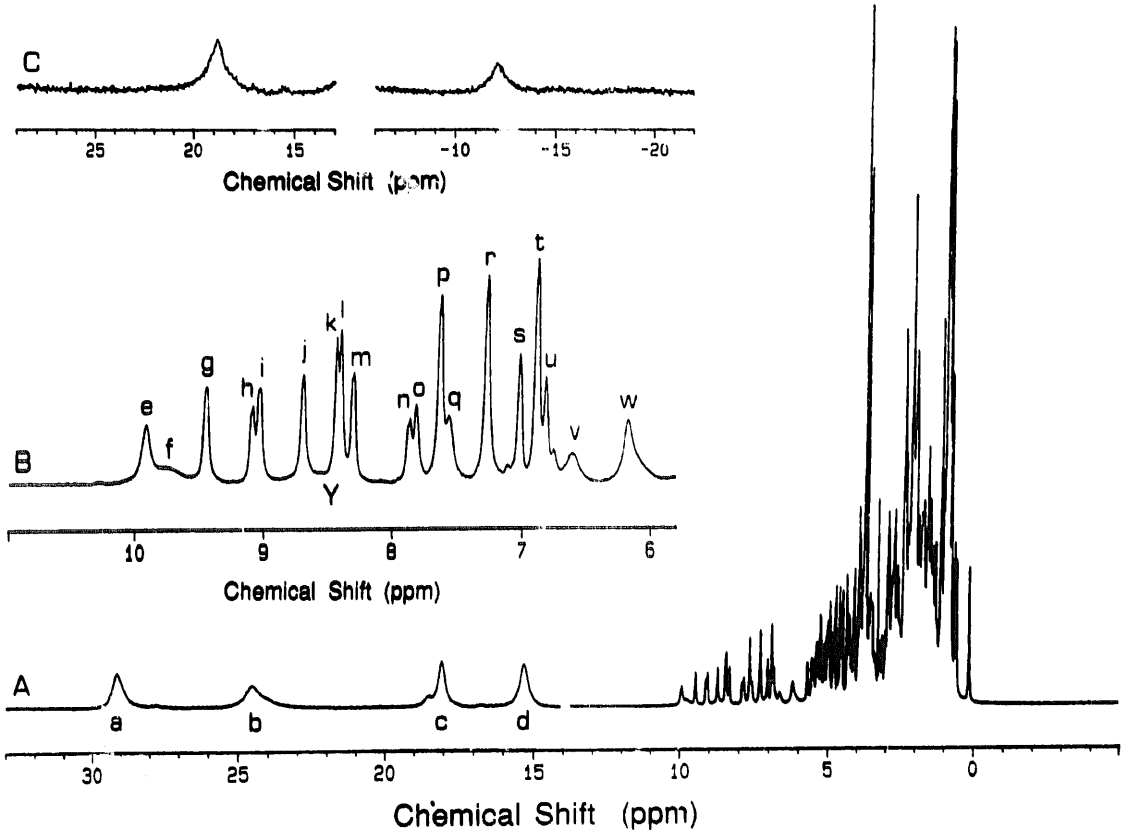

Fig. 5.12. 1H NMR spectrum of oxidized *D. gigas* ferredoxin II [35]. The two most downfield-shifted signals belong to a cysteine β-CH_2 pair experiencing Curie-type temperature dependence.

must be smaller than S_3; the total spin is $S' = \frac{1}{2}$, and S'_{12} from Mössbauer results to be equal to 2 [28], i.e. S_1 and S_2 are not completely antiferromagnetically coupled.

The spectrum of a protein containing such a cluster is reported in Fig. 5.12 [35]. There are four signals downfield which are assigned to one β-CH_2 pair of the cysteine

bound to iron 3 and to one β-CH_2 proton for each of the two cysteines bound to irons 1 and 2. The geminal protons of the latter are found in the diamagnetic region. The β-CH_2 pair of the cysteine coordinated to iron 3 ($S = \frac{5}{2}$) experiences a Curie temperature dependence, whereas the other four β-CH_2 protons are antiCurie, in agreement with their belonging to the cysteines coordinated to the $S'_{12} = 2$ pair which is smaller than $S_3 = \frac{5}{2}$. Other proteins containing Fe_3S_4 clusters have similar NMR properties [36].

5.4.2. *The $[(RS)_{11}Co_4]^{3-}$ case*

The protein metallothionein (MT) has a MW of 6000 and is rich in thiolate groups. It binds up to seven zinc(II), cadmium(II) and cobalt(II) ions. The seven ions are organized in two clusters. The so-called M_4S_{11} cluster is shown in Fig. 5.13. As suggested from X-ray and NMR measurements, metals 1 and 4 are coordinated by two terminal and two bridging cysteines, whereas metals 2 and 3 are coordinated by one terminal and three bridging cysteines [37–40]. As a consequence, $J_{14} = 0$. If the ions are antiferromagnetically coupled, metals 2 and 3 are overall more antiferromagnetically coupled than metals 1 and 4. This is going to explain some features of the NMR spectra [41,42]. Indeed, it has been proposed that the spectrum of Co_7MT shown in Fig. 5.14 is due only to the Co_4S_{11} cluster. This conclusion is reached on the basis of titration of the apoprotein with cobalt(II) and comparison with the Cd_4Co_3MT species. The spectrum is fascinating, in that signals are spread over

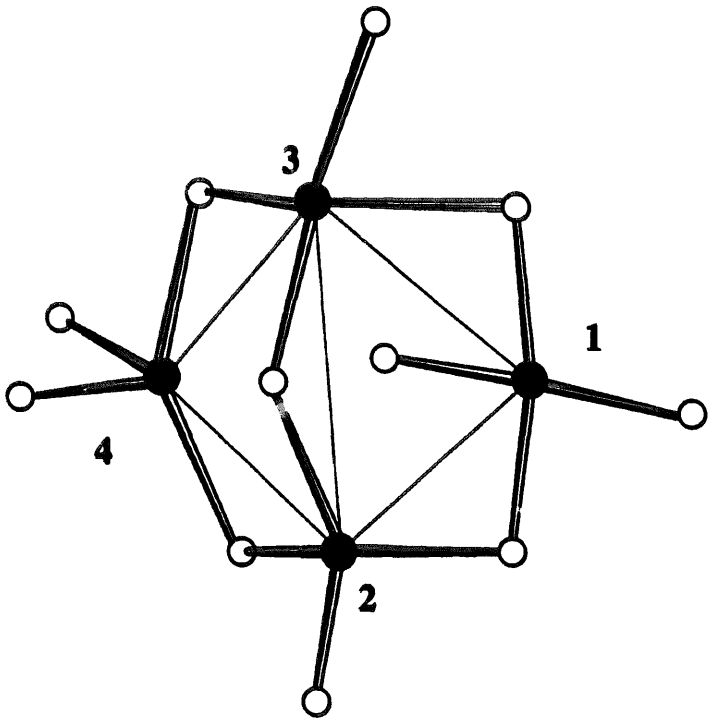

Fig. 5.13. Schematic structure of the M_4S_{11} cluster in metallothioneins (M = Zn, Cd, Co) [37–40]. There is no bridging ligand between metal 1 and metal 4.

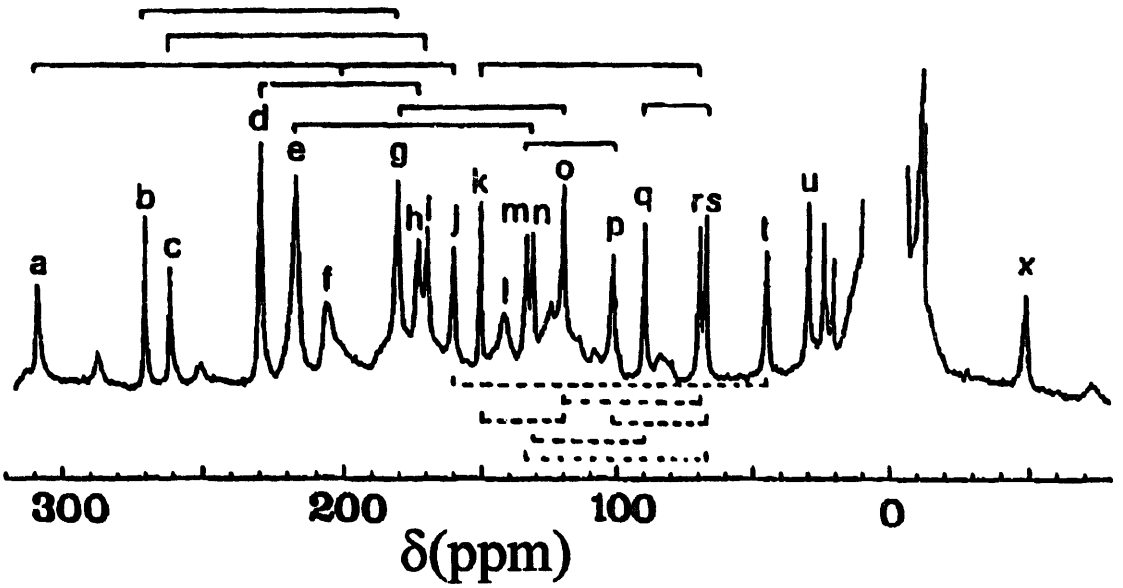

Fig. 5.14. ^{1}H NMR spectrum of Co_7MT showing the signals of the Co_4S_{11} cluster. The pairwise assignment of the β-CH_2 protons, obtained through NOE and NOESY is also shown [41–43].

400 ppm. The pairwise nature of nine out of 11 cysteine β-CH_2s has been demonstrated through NOE and NOESY [43] (see Sections 6.1 and 7.3). The connected signals are shown in Fig. 5.14.

The temperature dependence of the shifts shows that most of the signals follow a Curie-like behavior, whereas six signals (k, m, p, q, r, s) exhibit a more or less pronounced antiCurie behavior. The ground state of the system is $S' = 0$, since four equal ions are antiferromagnetically coupled. With a J of about 50 cm^{-1} several excited levels are occupied in the investigated range of temperature. If all the J values were equal we would expect an antiCurie behavior of all the signals. If one J value (namely J_{14}) is zero, we expect, from calculations performed using either Hamiltonian (5.19) or (5.22), the four terminal cysteines bound to metals 1 and 4 to exhibit normal Curie behavior; the two terminal cysteines bound to metals 2 and 3, and the cysteine bridging metals 2 and 3 to exhibit antiCurie behavior; and the four cysteines bridging metals 1 and 2, 1 and 3, 2 and 4, and 3 and 4 to experience contrasting effects, and thus to have a less pronounced temperature dependence (Fig. 5.15). As already mentioned, there are indeed six signals exhibiting antiCurie behavior [41,42].

5.4.3. *The $[(RS)_4Fe_4S_4]^{2-}$ case*

The $[(RS)_4Fe_4S_4]^{2-}$ case is encountered as inorganic compounds with other thiolate ligands and in proteins. The four iron atoms and the four sulfur atoms occupy the vertices of a cube (see Fig. 5.16). The tetracoordination of iron is reached through coordination to a further sulfur atom of a cysteine provided by the protein or of an organic thiolate in model complexes. Formally the cluster is constituted by

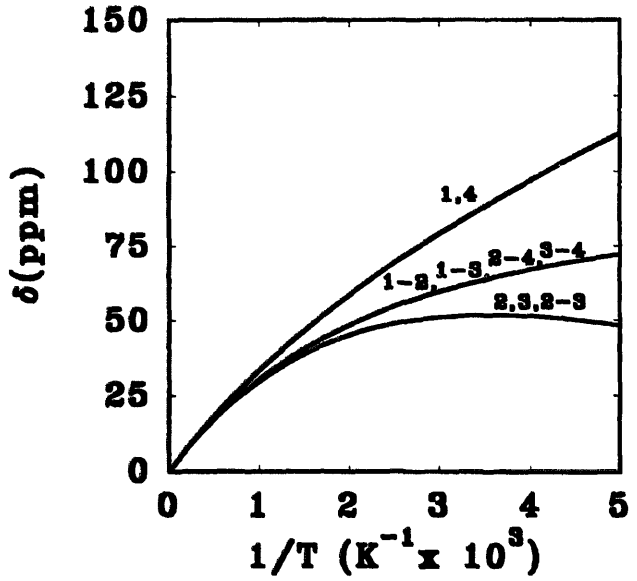

Fig. 5.15. Calculated hyperfine shifts for cysteine β-CH_2 protons of the Co_4S_{11} cluster from a magnetic coupling model with $J_{14}=0$ and all other J values equal to 50 cm^{-1}. Numbers refer to the metals to which the cysteines are coordinated (bridging cysteines being identified by two numbers).

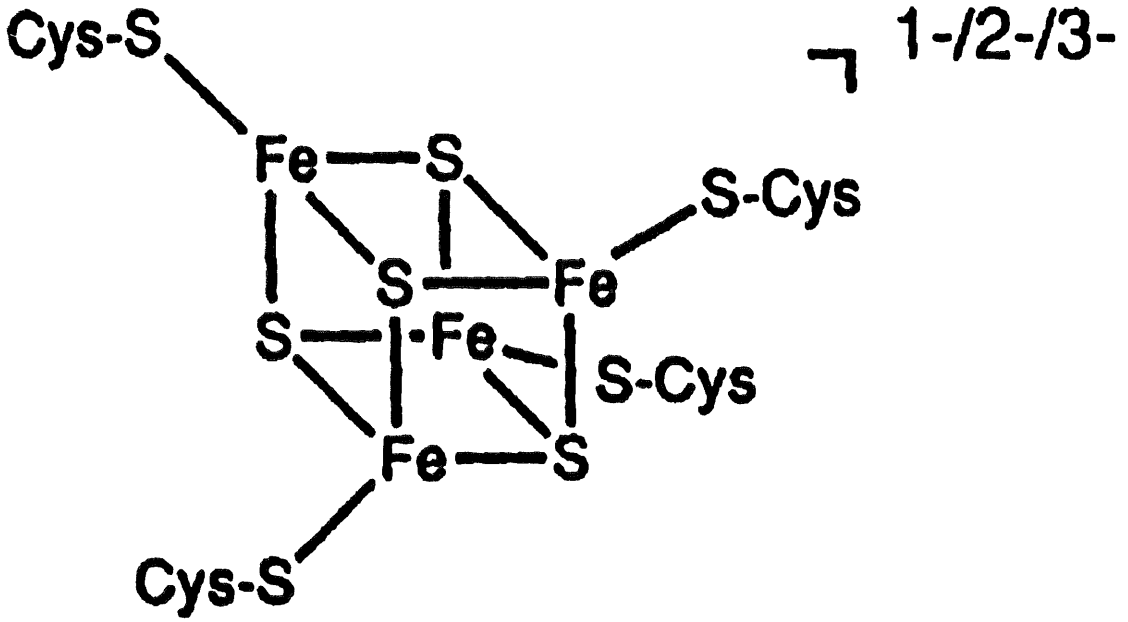

Fig. 5.16. Cubane-type Fe_4S_4 cluster. The total charge can be +3, +2, or +1 depending on the oxidation states of the iron ions. The cluster shown in the figure is coordinated to four protein cysteines, giving total charge of −1, −2 or −3 respectively.

two iron(III) and two iron(II) ions; actually Mössbauer spectroscopy showed that all iron ions are equivalent [44] and that the oxidation number is 2.5. The ground state is $S'=0$, but magnetically active states are populated at room temperature. The experimental temperature dependence of the shifts is of antiCurie type. NMR

has shown that the organic thiolate ligand exchanges fast on the time scale of the difference in shift between the various positions. Only one signal for the CH_2 protons of ethyl thiolate is observed [45,46]. In the case of proteins the rigidity of the ligand makes the two protons distinguishable. As discussed in Section 2.4, the shifts depend on the dihedral angles between the Fe–S–C and the S–C–H planes. NOE, NOESY and COSY spectra are available which show the connectivities between the β-CH_2 protons, and between the latter and the α-CH, as well as with various aminoacidic residues [47,48].

5.4.4. The $[(RS)_4Fe_4S_4]^-$ case

This cluster formally contains three iron(III) and one iron(II). It is present in a class of proteins called high potential iron–sulfur proteins (HiPIP). It has also been prepared through oxidation of $[(RS)_4Fe_4S_4]^{2-}$ model compounds [49]. Both in the model compound at low temperatures and in proteins we know that there is electron delocalization on one mixed valence pair [50–54]. Therefore, the polymetallic center is constituted by two iron ions at the oxidation state +2.5 and two iron ions at the oxidation state +3. Hamiltonian (5.19), or a more complicated one [33,55], can be used to describe the electronic structure. Indeed, a delocalization operator is sometimes needed in the Hamiltonian [33,55]. Consistently with magnetic Mössbauer data the S'_{34} subspin involving the mixed valence pair is $\frac{9}{2}$, whereas the S'_{12} subspin involving the iron(III) ions is 4. Mössbauer and EPR data do not exclude $\frac{7}{2}$ and 3 respectively for the two pairs [49]; in any case, the subspin value of the mixed valence pair is larger than that of the iron(III) pair. This information is vital for the interpretation of the NMR spectra. The β-CH_2 of the cysteines of the mixed valence domain go downfield because they sense the larger spin, whereas the β-CH_2 protons of the cysteines of the iron(III) domain are upfield. Note the similarity with the reduced Fe_2S_2 case (see Section 5.3.4). The total spin of the ground state is $S' = \frac{1}{2}$, and levels with larger S' values are available at room temperature. The T_1 values of the hyperfine shifted signals are accordingly quite short (4–25 ms). The spectrum of the oxidized HiPIP II from *E. halophila* is shown in Fig. 5.17(A). The β-CH_2 protons are pairwise assigned through NOEs. The picture is absolutely consistent with what is discussed above [56]. The temperature dependence is consistent with expectations (Fig. 5.18). It should be noted now that electron delocalization may require a further operator in Hamiltonian (5.19). Its introduction may be relevant for the interpretation of fine aspects of oxidized HiPIPs, but we deliberately avoid this further treatment [32].

The next step in the knowledge of the protein structure is that of identifying the cysteines bound to the two kinds of iron ions. This goal is reached with the procedures illustrated in the next chapters.

5.4.5. The $[(RS)_4Fe_4S_4]^{3-}$ case

This center formally contains three iron(II) and one iron(III) ions. The Mössbauer data indicate that in most cases we are in the presence of two irons at the oxidation

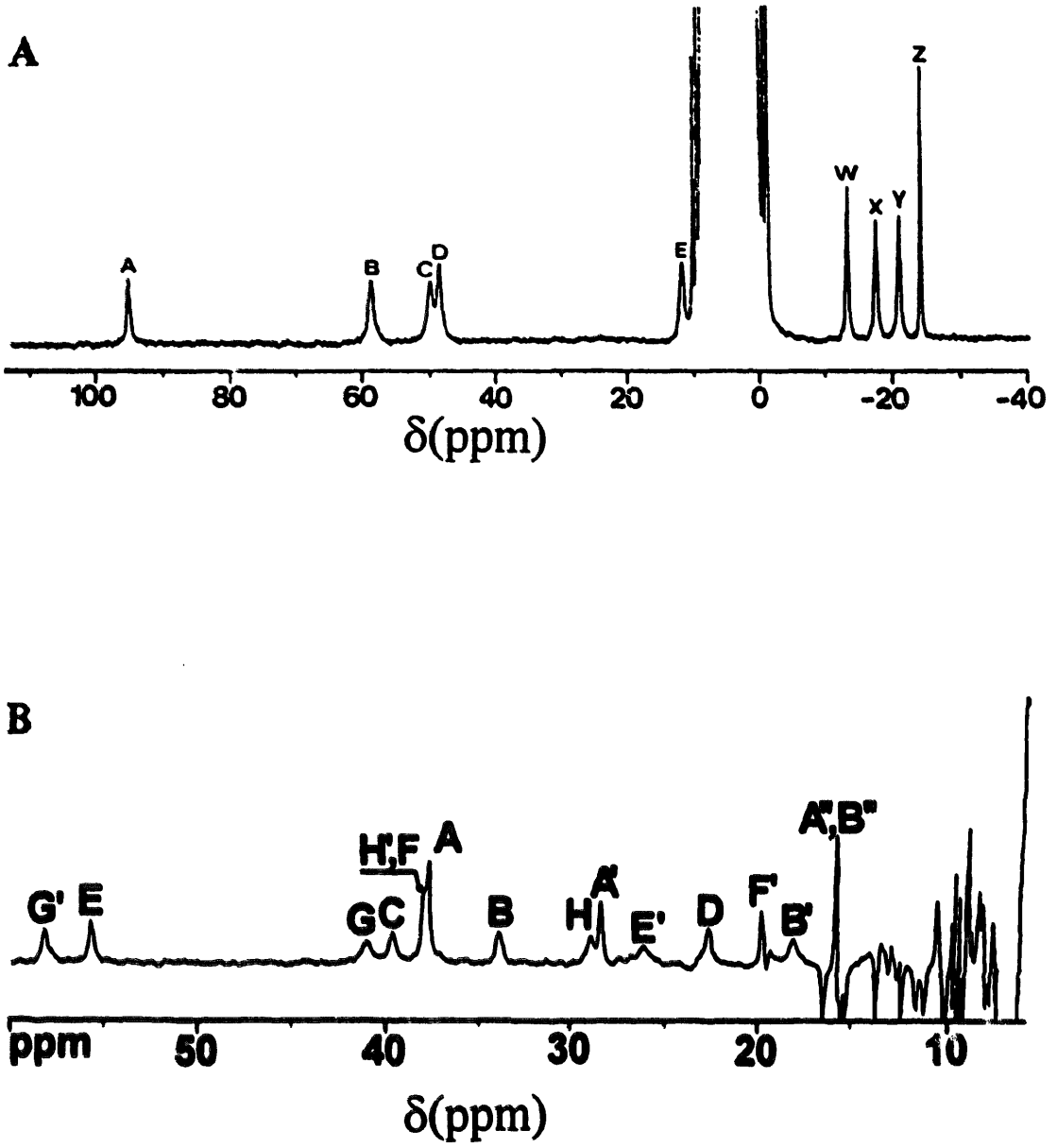

Fig. 5.17. ^{1}H NMR spectra of (A) oxidized HiPIP II from *E. halophila* [56] and (B) reduced ferredoxin from *C. acidi urici* [48].

state +2.5 and two irons at the oxidation state +2 [57–59]. The system is present in ferredoxins and has been synthesized as model compounds. The ground state in proteins seems to be $\frac{1}{2}$. The ^{1}H NMR spectrum of the two reduced clusters present in *C. acidi urici* ferredoxin is shown in Fig. 5.17(B). Note the differences in chemical shifts with respect to Fig. 5.17(A); such differences are attributed to different degrees of electron delocalization. In reduced Fe_4S_4 ferredoxins the shifts are all downfield, half of them with Curie and half with antiCurie temperature dependence, just like in the case of the reduced Fe_2S_2 ferredoxins discussed in Section 5.3.4. The successful strategy for the investigation of these systems [47,48] is similar to that of the oxidized

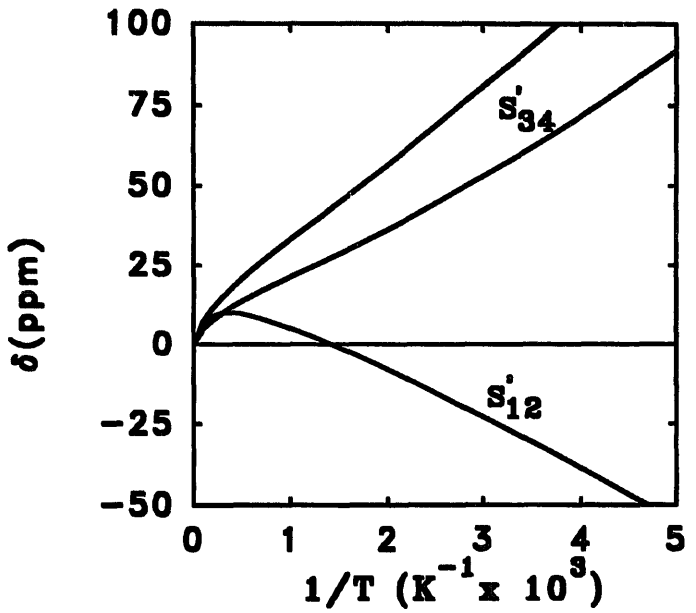

Fig. 5.18. Experimental and calculated temperature dependence of the hyperfine shifts of the cysteine β-CH_2 protons of HiPIP II from *E. halophila* [56]. S'_{12} refers to the protons sensing the ferric pair and S'_{34} to those sensing the mixed valence pair.

HiPIPs. In model compounds both $\frac{1}{2}$ and $\frac{3}{2}$ ground states have been found [60]. When S is substituted with Se a $\frac{7}{2}$ ground state has been claimed [61]. Surely there will be fun in the investigation of these systems by NMR.

5.4.6. *The $[(RS)_3LFe_3NiS_4]^{3-}$ case*

In this case one iron(II) has been substituted by a nickel(II) ion. As a model complex this is a nice system to investigate [62]. Reports are available which show that such polymetallic centers are embedded in proteins [63]. In the model complex a triphenylphosphine is bound to nickel (if L is a neutral ligand the negative charge of the title compound should be decreased by one unit). Interestingly, the shift pattern of the triphenylphosphine moiety is reversed with respect to a nickel(II) complex without magnetic coupling [62]. This can be seen as the result of a spin $S' = \frac{5}{2}$, resulting from the Fe_3S_4 moiety, antiferromagnetically coupled to $S = 1$ of nickel(II). Alternatively, the $S' = \frac{9}{2}$ of the iron(III)–iron(II) mixed valence pair is antiferromagnetically coupled to the iron(II)–nickel(II) pair [64].

This system has been chosen just to pinpoint the variety of systems and of spin coupling schemes available in heteropolymetallic systems.

References

[1] A. Bencini and D. Gatteschi, Electron Paramagnetic Resonance of Exchange-Coupled Systems, Springer, Berlin, 1990.

[2] W.R. Dunham, G. Palmer, R.H. Sands and A.J. Bearden, Biochim. Biophys. Acta, 253 (1971) 373.
[3] L. Banci, I. Bertini and C. Luchinat, Struct. Bonding, 72 (1990) 113.
[4] C. Luchinat and S. Ciurli, Biol. Magn. Res., 12 (1993) 357.
[5] I. Bertini, L. Banci, R.D. Brown III, S.H. Koenig and C. Luchinat, Inorg. Chem., 27 (1988) 951.
[6] J.A. Tainer, E.D. Getzoff, K.M. Beem, J.S. Richardson and D.C. Richardson, J. Mol. Biol., 160 (1982) 181.
[7] I. Bertini, O. Galas, C. Luchinat and G. Spina, unpublished results, 1996.
[8] A.G. Redfield, Res. Dev. 1 (1957) 19.
[9] W.J. Stratton, Inorg. Chem., 9 (1970) 517.
[10] P.D.W. Boyd, M. Gerlock and G.M. Sheldrick, J. Chem. Soc. Dalton Trans., (1974) 1097.
[11] D. Gatteschi, A. Dei and E. Piergentili, Inorg. Chem., 18 (1979) 89. C. Benelli, A. Dei and D. Gatteschi, Inorg. Chem., 108 (1982) 3298.
[12] C. Owens, R.S. Drago, I. Bertini, C. Luchinat and L. Banci, J. Am. Chem. Soc., 108 (1986) 3298.
[13] I. Bertini, C. Luchinat, C. Owens and R.S. Drago, J. Am. Chem. Soc., 109 (1987) 5208.
[14] W. Byers and R.J.P. Williams, J. Chem. Soc., 11 (1973) 134.
[15] M. Maekawa, S. Kitagawa, M. Munakata and H. Masuda, Inorg. Chem., 28 (1989) 1904.
[16] G.N. La Mar, G.R. Eaton, R.H. Holm and F.A. Walker, J. Am. Chem. Soc., 95 (1973) 63.
[17] M. Poe, W.D. Phillips, J.D. Glickson, C.C. McDonald and A. San Pietro, Proc. Natl. Acad. Sci. USA, 68 (1971) 68.
[18] I. Saalmen and G. Palmer, Arch. Biochem. Biophys., 150 (1972) 767.
[19] I. Morgenstern-Badarau, D. Cocco, A. Desideri, G. Rotilio, J. Jordanov and N. Dupré, J. Am. Chem. Soc., 108 (1986) 300.
[20] I. Bertini, C. Luchinat and M. Piccioli, Progr. Nucl. Magn. Reson. Spectrosc., 26 (1994) 91.
[21] I. Bertini, C. Luchinat, L.J. Ming, M. Piccioli, M. Sola and J.S. Valentine, Inorg. Chem., 31 (1992) 4433.
[22] I. Bertini, G. Lanini, C. Luchinat, L. Messori, R. Monnanni and A. Scozzafava, J. Am. Chem. Soc., 107 (1985) 4391.
[23] L. Banci, I. Bertini, C. Luchinat and A. Scozzafava, J. Am. Chem. Soc., 109 (1987) 2328.
[24] L. Banci, I. Bertini, C. Luchinat, R. Monnanni, A. Scozzafava and B. Salvato, Gazz. Chim. Ital., 116 (1986) 51; L. Banci, I. Bertini, C. Luchinat, R. Monnanni and A. Scozzafava, Inorg. Chem., 26 (1987) 153.
[25] I. Bertini, G. Lanini and C. Luchinat, Inorg. Chem., 23 (1984) 2729.
[26] L. Skjeldal, J.L. Markley, V.M. Coghlan and L.E. Vickery, Biochemistry, 30 (1991) 9078.
[27] L.B. Dugad, G.N. La Mar, L. Banci and I. Bertini, Biochemistry, 29 (1990) 2263.
[28] T.A. Kent, B.H. Huynh and E. Munck, Proc. Natl. Acad. Sci. USA, 77 (1980) 6574.
[29] L. Noodleman, Inorg. Chem., 27 (1988) 3677.
[30] L. Noodleman, Inorg. Chem., 30 (1991) 256.
[31] L. Noodleman, Inorg. Chem., 30 (1991) 246.
[32] I. Bertini, S. Ciurli and C. Luchinat, in Structure and Bonding, Vol. 83, Springer, Berlin, Heidelberg, 1995, pp. 1–54.
[33] G. Blondin and J.-J. Girerd, Chem. Rev., 90 (1990) 1359. E.L. Bominaar, S.A. Borshch and J.-J. Girerd, J. Am. Chem. Soc., 116 (1994) 5362; 116 (1994) 7957.
[34] I. Bertini, F. Briganti and C. Luchinat, Inorg. Chim. Acta, 175 (1990) 9.
[35] A.L. Macedo, I. Moura, J.J.G. Moura, J. LeGall and B.H. Huynh, Inorg. Chem., 32 (1993) 1101.
[36] S.C. Busse, G.N. La Mar, L.P. Yu, J.B. Howard, E.T. Smith, Z.H. Zhou and M.W.W. Adams, Biochemistry, 31 (1992) 11952.
[37] A. Arseniev, P. Schultze, E. Worgotter, W. Braun, G. Wagner, M. Vasak, J.H. Kagi and K. Wüthrich, J. Mol. Biol., 201 (1988) 637.
[38] P. Schultze, E. Worgotter, W. Braun, G. Wagner, M. Vasak, J.H.R. Kägi and K. Wüthrich, J. Mol. Biol., 203 (1988) 251.
[39] B.A. Messerle, A. Schaeffer, M. Vasak, J.H.R. Kägi and K. Wüthrich, J. Mol. Biol., 214 (1990) 765.
[40] A.H. Robbins, D.E. McRee, M. Williamson, S.A. Collett, X.H. Xuong, W.F. Furey, B.C. Wang and C.D. Stout, J. Mol. Biol., 221 (1991) 1269.
[41] I. Bertini, C. Luchinat, L. Messori and M. Vasak, J. Am. Chem. Soc., 111 (1989) 7296.

[42] I. Bertini, C. Luchinat, L. Messori and M. Vasak, J. Am. Chem. Soc., 111 (1989) 7300.
[43] I. Bertini, C. Luchinat, L. Messori and M. Vasak, Eur. J. Biochem., 211 (1993) 235.
[44] R. Cammack and A.G. Sykes (Eds.), Advances in Inorganic Chemistry. Iron–Sulfur Proteins, Academic Press, San Diego, 1992.
[45] K.S. Hagen, A.D. Watson and R.H. Holm, J. Am. Chem. Soc., 105 (1983) 3905.
[46] R.H. Holm, W.D. Phillips, B.A. Averill, J.J. Mayerle and T. Herskovitz, J. Am. Chem. Soc., 96 (1974) 2109.
[47] I. Bertini, F. Briganti, C. Luchinat, L. Messori, R. Monnanni, A. Scozzafava and G. Vallini, Eur. J. Biochem., 204 (1992) 831.
[48] I. Bertini, F. Capozzi, C. Luchinat, M. Piccioli and A.J. Vila, J. Am. Chem. Soc., 116 (1994) 651.
[49] J.M. Mouesca, G.J. Rius and B. Lamotte, J. Am. Chem. Soc., 115 (1993) 4714.
[50] P. Middleton, D.P.E. Dickson, C.E. Johnson and J.D. Rush, Eur. J. Biochem., 104 (1980) 289.
[51] D.P.E. Dickson, C.E. Johnson, R. Cammack, M.C.W. Evans, D.O. Hall and K.K. Rao, Biochem. J., 139 (1974) 105.
[52] I. Bertini, A.P. Campos, C. Luchinat and M. Teixeira, J. Inorg. Biochem., 52 (1993) 227.
[53] V. Papaefthymiou, M.M. Millar and E. Munck, Inorg. Chem., 25 (1986) 3010.
[54] J. Gloux, P. Gloux, B. Lamotte, J.M. Mouesca and G.J. Rius, J. Am. Chem. Soc., 116 (1994) 1953.
[55] M. Belinskii, I. Bertini, O. Galas and C. Luchinat, Z. Naturforsch. Teil A:, 50 (1995) 75.
[56] L. Banci, I. Bertini, F. Capozzi, P. Carloni, S. Ciurli, C. Luchinat and M. Piccioli, J. Am. Chem. Soc., 115 (1993) 3431.
[57] P. Middleton, D.P.E. Dickson, C.E. Johnson and J.D. Rush, Eur. J. Biochem., 88 (1978) 135.
[58] R.N. Mullinger, R. Cammack, K.K. Rao, D.O. Hall, D.P.E. Dickson, C.E. Johnson, J.D. Rush and A. Simonopulos, Biochem. J., 151 (1975) 75.
[59] D.P.E. Dickson, C.E. Johnson, P. Middleton, J.D. Rush, R. Cammack, D.O. Hall, R.N. Mullinger and K.K. Rao, J. Phys. (Paris) Colloq., 37 (1976) C6-171.
[60] R.H. Holm, S. Ciurli and J.A. Weigel, in S.J. Lippard (Ed.), Progress in Inorganic Chemistry: Bioinorganic Chemistry, Vol. 38, Wiley, New York, 1990, pp. 1–74.
[61] J. Meyer, J.-M. Moulis, J. Gaillard and M. Lutz, Adv. Inorg. Chem., 38 (1992) 73.
[62] S. Ciurli, P.K. Ross, M.J. Scott, S.-B. Yu and R.H. Holm, J. Am. Chem. Soc., 114 (1992) 5415.
[63] M. Teixeira, I. Moura, A.V. Xavier, J.J.G. Moura, J. LeGall, D.V. DerVartanian, H.D. Peck, Jr. and B.H. Huynh, J. Biol. Chem., 264 (1989) 16435.
[64] I. Bertini and C. Luchinat, Chem. Tracts, 4 (1992) 269.